Journal of Drug Delivery Science and Technology 109 (2025) 107002

Contents lists available at ScienceDirect

Journal of Drug Delivery Science and Technology

journal homepage: www.elsevier.com/locate/jddst

Indomethacin microencapsulation by coaxial ultrasonic atomization intended for intraarticular administration

Iván Lamela-Gómez [a,b], Asteria Luzardo-Álvarez [a,b,*]

[a] Department of Pharmacology, Pharmacy and Pharmaceutical Technology, Faculty of Sciences, Universidade de Santiago de Compostela, Campus Terra, 27002, Lugo, Spain
[b] PARAQUASIL Group. Health Research Institute of Santiago de Compostela (IDIS), 15706, Santiago de Compostela, Spain

ARTICLE INFO

Keywords:
Indomethacin
Microencapsulation
NSAIDs
Intra-articular
Controlled release
Rheumatoid arthritis

ABSTRACT

Indomethacin (IND) is a non-steroidal anti-inflammatory drug (NSAID) with high efficacy in the treatment of rheumatic disorders. Nonetheless, its severe adverse effects limit its first-line and long-term use, and its rapid clearance from the joint prevents its local administration. This study aims to overcome those limitations by developing an intra-articular formulation of IND-loaded microparticles made of polymeric blends of Polyactive® 1000PEOT70PBT30 and Resomer® RG502. Formulations were prepared by coaxial ultrasonic atomization according to an experimental design to assess the influence of the polymeric composition and flow rates supplied to the nozzle over particle size, encapsulation efficiency and *in vitro* delivery profile. Nine formulations of spherical microparticles were developed and exhaustively characterized, showing high drug entrapment (56.2–81.32 %) and suitable mean particle size for intra-articular administration (22.8–82.6 μm). *In vitro* evaluation of IND-loaded microparticles in THP-1 macrophages demonstrated their biocompatibility and extensive internalization by THP-1 cells, supporting their potential for macrophage targeting and particle retention into the joint. Further, IND-loaded microparticles showed high anti-inflammatory activity *in vitro,* significantly reducing the production of IL-6 and TNF-α by LPS-stimulated macrophages. Overall, the results support the idea that IND-loaded microcapsules are a suitable drug delivery system for the intra-articular administration of indomethacin.

1. Introduction

Indomethacin (2-[1-(4-chlorobenzoyl)-5-methoxy-2-methylindol-3-yl] acetic acid; IND) (Fig. 1) is a non-selective non-steroidal anti-inflammatory drug (NSAIDs), exhibiting a higher potency than other widely used NSAIDs like naproxen, ibuprofen and acetylsalicylic acid. Since its first approval by FDA in 1965, it has been widely used with high efficacy in the treatment of several pathologies, mainly in the therapeutical management of moderate to severe rheumatic disorders, including rheumatoid arthritis, osteoarthritis and gouty arthritis [1,2].

Although its high efficacy, the use of IND as a first-line and long-term therapy is limited by its adverse effects, mainly dose-dependent, which affect 30–60 % of patients and lead to a high treatment discontinuation rate (10–20 %). Its adverse effects profile includes severe gastrointestinal injury, severe renal toxicity<, neurologic effects and hematologic disorders.Therefore, it's necessary to continue developing innovative dosage forms and explore alternative administration routes to improve indomethacin's efficacy and security profile [3–5].

Rheumatoid arthritis (RA) is an autoimmune inflammatory disease characterized by chronic inflammation of the synovial membrane, which courses with chronic pain, joint stiffness and disabling arthritis, severely affecting the patient's quality of life. With a prevalence ranging between 0.5 and 1 %, established RA has a tremendous social impact and health expenditure [6].

Pharmacological therapy of RA often comprises the systemic administration of a combination of disease-modifying anti-rheumatic drugs (DMARDs), corticosteroids, and non-steroidal anti-inflammatory drugs. The development of biological anti-TNF-α DMARDs such as Infliximab, Adalimumab or Golimumab significantly improved the systemic managment of RA, allowing for long-term remission rates of RA patients [7]. Nonetheless, intra-articular (IA) administration of corticosteroids and NSAIDs to treat acute episodes and relapses is frequently employed in the clinical practise. The direct drug delivery into the joint allows us to achieve a high drug concentration on the site of

* Corresponding author. Department of Pharmacology, Pharmacy and Pharmaceutical Technology, Faculty of Sciences, Universidade de Santiago de Compostela, Campus Terra, 27002, Lugo, Spain.
E-mail address: asteriam.luzardo@usc.es (A. Luzardo-Álvarez).

https://doi.org/10.1016/j.jddst.2025.107002
Received 16 December 2024; Received in revised form 1 May 2025; Accepted 2 May 2025
Available online 5 May 2025

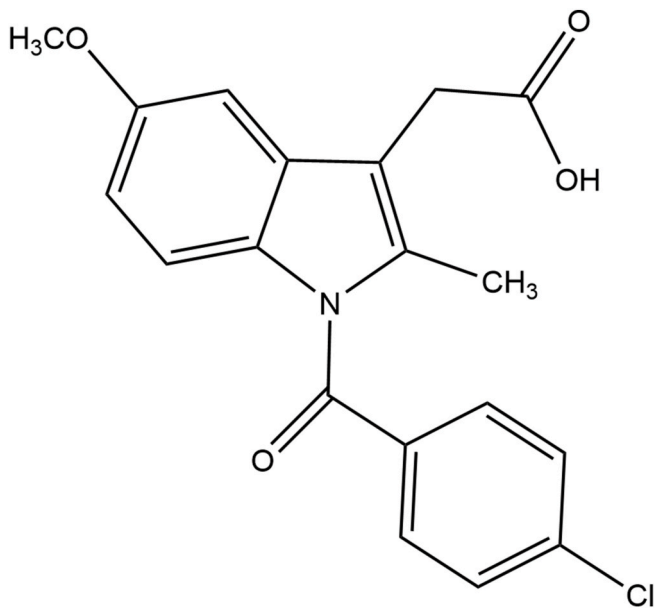

Fig. 1. Chemical structure of Indomethacin.

inflammation and reduce its systemic toxicity, providing a rapid anti-inflammatory effect and pain relief [8–11]. Despite all the potential advantages of IA injection, its use as a long-term administration route is limited due to the high articular clearance rate of most drugs, making necessary frequent injections, which are not well tolerated and can increase the risk of infection [12]. Concisely, after the IA injection of a 10 mg single dose of indomethacin, the drug was rapidly cleared from the joint, showing a mean articular residence time of 4 h. Moreover, the maximum plasmatic concentration of IND was reached 1 h after IA administration, exhibiting an 80 % systemic bioavailability. Also, no significant differences were found in AUC and half-life after intra-articular or intravenous administration of IND [13].

These limitations have stimulated the development of novel drug delivery systems designed to increase drug retention at the joint cavity [14], and to achieve a sustained release profile of IND at the site of action, thus potentially increasing its efficacy and minimizing its systemic adverse effects. In this context, several approaches have been explored, including different drug clases and technological approaches. Different microparticulate formulations based on PLGA were investigated for intra-articular delivery of corticosteroids such as triamcinolone [15,16], dexamethasone [17] or mometasone [18], leading to a increase in the drug residence time into the joint. This local treatment approach based on polymeric microparticles showed also promising results *in vitro* for NSAIDs (Celecoxib and etoricoxib) [19,20], and biological DMARDs (Infliximab) [21]. Focusing on IND, several drug delivery systems were already explored to achieve its local delivery and retention into the joint, including micro- and nanoparticles [22,23], hydrogels [24], micelles [25] or nanoemulsions [26]. In this work, we explored an approached based on the excellent properties of microencapsulation to developing a drug delivery system with convenient features to be retained in the articular space and to achieve therapeutical levels of IND in the joint long-term, taking into account that particle size is a crucial factor in achieving effective retention in inflamed, highly permeable joints, agreeing with data previously reported [27,28]. Concisely, Pradal et al. found in an *in vivo* mouse model that nanoparticles smaller than 250 nm are quickly cleared from the joint space, while effective retention of particles is achieved for particles larger than 10 μm [29].

This work aims to develop and characterize indomethacin-loaded polymeric microcapsules with suitable properties for intra-articular administration. Microparticles were prepared by ultrasonic coaxial atomization using different mixtures of Polyactive® 1000PEOT70PBT30 and Resomer® RG502 as shell-forming polymers. The influence of the polymeric composition and formulation parameters were evaluated according to an experimental design. The formulations obtained were exhaustively characterized in terms of pharmaceutical properties and *in vitro* biological response *in* cell cultures.

2. Materials and methods

2.1. Materials

Polyactive® 1000PEOT70PBT30 (PEOT-PBT) multiblock copolymer with a 30 wt% of poly(ethylene-oxide-terephthalate) (PEOT; Mw = 1000 Da) and a 70 wt% of poly(butylene-terephthalate) (PBT) was purchased from PolyVation® (Groningen, The Netherlands). Ester end-capped PLGA [Poly-(D, L-lactide-*co*-glycolide)] (Resomer® RG 502; Mw = 7000–17000 Da) with a 50:50 co-polymerization rate was obtained from Boehringer Ingelheim (Ingelheim, Germany). Indomethacin (IND) was obtained from Guinama (Valencia, Spain). PVA (Poly (vinyl alcohol); Mw = 30,000–70,000 Da), Coumarin-6, DAPI (4′,6-Diamidino-2-phenylindole dihydrochloride), DAPI (4′,6-Diamidino-2-phenylindole dihydrochloride) and *E. coli* lipopolysaccharide (LPS) was supplied by Sigma-Aldrich (Madrid, Spain). Methylene chloride, methanol and formaldehyde were purchased from PanReac AppliChem (Barcelona, Spain). All solvents were HPLC grade, whereas all other reagents were of analytical grade. Phenazine methosulfate (PMS) was supplied by Acros Organics (Geel, Belgium) and XTT sodium salt by Alfa Aesar (Kandel, Germany). Phorbol 12-myristate 13-acetate (PMA), phalloidin, specific antibody pairs and all reagents necessary to perform ELISA were supplied by Abcam (Cambridge, United Kingdom). Culture medium, foetal bovine serum (FBS), trypsin/EDTA and all supplements to cell culture were purchased from Biological Industries (Cromwell, CT, USA).

2.2. Preparation of microparticles

Indomethacin-loaded microparticles (IND-MPs) were fabricated using a dual-feed coaxial ultrasonic nozzle equipped with a power supply operated at fixed frequency (60 KHz) and variable power. (Sono-Tek Corp., Milton, USA). The inner and the outer channel were fed, respectively, by a programmable syringe pump (NE-1000; New Era Pump Systems Inc, Farmingdale, USA) and a variable flow rate Merck-Hitachi L6000 pump (Merck-Hitachi, Tokyo, Japan). Briefly, a 3 % (w/w) polymeric blend solution in CH_2Cl_2 containing a mixture of 1000PEOT70PBT30 and Resomer® RG502 (PLGA502) at different ratios was infused through both channels at a total flow rate of 1 ml/min, obtaining a fine spray which was collected over a 2 % (w/w) PVA stirring solution. The appropriate amount of indomethacin to achieve a theoretical drug loading of 0.1 g of drug per gram of polymer was dissolved into the polymeric solution atomized through the inner channel, whereas the outer solution remained drug-free. Power was fixed at 4 Watts for all the microparticle formulations prepared, whereas the PEOT-PBT/PLGA502 ratio and the contribution of each channel to the total flow rate (1 ml/min) were set accordingly to a statistical experimental design. After atomization, the solvent was evaporated under magnetic stirring at room temperature for 4 h. Afterwards, microparticles (MPs) were isolated by filtration, washed twice with deionized water, and dried in a vacuum chamber. The whole process was performed under subdued light to prevent the degradation of indomethacin.

2.3. Experimental design

To assess the influence of the polymeric composition and flow rate on the morphology, particle size, encapsulation efficiency and *in vitro* drug delivery rate of the microparticles, a statistical experimental design was built using Statgraphics Centurion 18 software, v.18.1.12 (Statgraphics Technologies, Inc., The Plains, VA, USA). A central composite rotatable

and orthogonal design was selected, including 9 different formulations with 8 replicates of the central point. The limits for PLGA502 content in the PEOT-PBT/PLGA502 polymeric blend were set between 14.64 and 85.36 %, and the flow rate through the external channel was set between 0.22 and 0.78 ml/min, maintaining a total flow rate of 1 ml/ml through both channels (Table 1). The 16 formulations contained in the experimental design were prepared in random order.

Experimental data obtained after the characterization of the microparticles were fitted to a quadratic multiple regression model to evaluate the influence of the formulation parameters over particle size, encapsulation efficiency and drug delivery rate. Equation (1) describes the quadratic model, where A is the percentage of PLGA502 in the polymer mixture, B is the flow rate through the outer channel, and *a, b, c, d, e*, and *k* are the regression coefficients. Finally, optimal formulations were selected by surface response methodology. Graphical and statistical analysis was performed with Statgraphics Centurion 18 statistical package.

$$\text{Response Variable} = a\cdot A + b\cdot B + c\cdot A^2 + d\cdot B^2 + e\cdot A\cdot B + k \quad (1)$$

2.4. Process yield and encapsulation efficiency

Drug loading was calculated for all formulations obtained. To completely extract indomethacin from the microparticles, 10 mg of dry MPs were accurately weighed into a 10 ml volumetric flask and dissolved in 500 μl of methylene chloride. Subsequently, methanol was slowly added up to 10 ml to precipitate the polymer and solubilize the indomethacin contained in microparticles, and then the precipitated polymer was removed by filtration through a 0.45 μm nylon syringe filter. Finally, the methanolic solution was 5-fold diluted, and indomethacin concentration (μg/ml) was determined spectrophotometrically at the maximum absorption wavelength (λ = 318 nm). For quantification, standard solutions of IND in methanol with a concentration ranging between 0.78 and 100 μg/ml were prepared in triplicate and analyzed at the maximum absorption wavelength (λ = 318 nm) using an Evolution 60 s UV–Vis spectrophotometer (Thermo Fisher Scientific, Waltham, MA, USA). Collected data were analyzed by linear regression leading to the following calibration curve: $A_{318\,nm} = (0.02408 \pm 0.00362) + (0.01660 \pm 0,00008)\cdot[IND]$ $(R^2 = 0.9999)$. The analytical method showed a good linearity, as shown the determination coefficient ($R^2 = 0.9999$). The detection limit (DL = 0.720 μg/ml) and limit of quantification (QL = 2.183 μg/ml) where estimated according to the validation protocols describes in QR(R2) ICH Guidelines [30]. Blank microparticles were also analyzed, verifying the absence of analytical interference. Finally, indomethacin's encapsulation efficiency (E.E.) was calculated according to Equation (2). Process Yield (P.Y.) was calculated following Equation (3).

$$E.E.\ (\%) = \frac{Real\ loaded\ Indomethacin}{Theoretical\ \ loaded\ indomethacin} \times 100 \quad (2)$$

$$P.Y.\ (\%) = \frac{Dry\ microcapsules\ weight}{Polymer\ weight + Drug\ weight} \times 100 \quad (3)$$

Table 1
Preparation parameters for all formulations included in the experimental design.

Formulation	Polymeric composition (%)		Flow rate (ml/min)	
	PLGA502	PEOT/PBT	Outer channel	Inner channel
F1	50.0	50.0	0.50	0.50
F2	50.0	50.0	0.78	0.22
F1	50.0	50.0	0.50	0.50
F3	14.6	85.4	0.50	0.50
F1	50.0	50.0	0.50	0.50
F4	75.0	25.0	0.70	0.30
F5	25.0	75.0	0.30	0.70
F1	50.0	50.0	0.50	0.50
F6	85.4	14.6	0.50	0.50
F7	75.0	25.0	0.30	0.70
F1	50.0	50.0	0.50	0.50
F1	50.0	50.0	0.50	0.50
F1	50.0	50.0	0.50	0.50
F1	50.0	50.0	0.50	0.50
F8	50.0	50.0	0.22	0.78
F9	25.0	75.0	0.70	0.30

2.5. Particle size analysis

Particle size distribution was measured by laser diffraction accordingly to the Fraunhofer diffraction model in a Mastersizer particle size analyzer (Malvern Instruments, Malvern, UK). An adequate amount of microparticles was resuspended in deionized water and sonicated for 1 min before analysis to disrupt aggregates and remove air bubbles. All samples were analyzed in triplicate, and results were expressed as volume-weighted size distribution, characterized by d(v,0.1), d(v,0.5) and d(v,0.9), which represent the diameter below which the 10 %, 50 % and 90 % of the size distribution lies. Surface-weighted (D [3,4]) and Volume-Weighted (D [2,3]) mean diameters were also reported. Further, Span was calculated according to Equation (4) as a size distribution width characteristic parameter.

$$Span = \frac{d(v,0.9) - d(v,0.9)}{d(v,0.5)} \quad (4)$$

2.6. ζ potential determination

ζ potential of the microparticles was assessed by electrophoretic light scattering (ELS). Briefly, dry MPs in powder form were resuspended in 1 mM KCl and sonicated for 30 s before measurement using a ζ potential analyzer (ZetaPlus, Brookhaven Instruments Corporation, New York, USA). Determinations were performed at 25 °C and pH 7. All samples were assayed in triplicate, and ten measurements were performed on each sample.

2.7. X-ray powder diffraction analysis (XRPD)

XRPD patterns were acquired using a Bruker D8 Advance X-ray diffractometer (Bruker Corporation, Billerica, MA, USA) equipped with a CuKα1 radiation source (λ = 1.5406 Å) and a Lynxeye XE-T detector. For analysis, dry samples were placed on a Si(511) sample holder and scanned in Brang-Brentano reflection mode from 2° to 50° 2θ, with a step size of 2° and a scanning speed of 0.6° per minute. Samples were also rotated during measurements to minimize the effect of the preferred orientation. The operation voltage and current were 40 kV and 40 mA, respectively. Finally, diffraction patterns were generated and analyzed using HighScore Plus (v.3.0) software package (Malvern Panalytical, Almelo, The Netherlands).

2.8. Differential Scanning Calorimetry

Thermal analysis of Indomethacin, Empty-MPs and IND-loaded MPs was performed by Differential Scanning Calorimetry (DSC). Briefly, around 5 mg of sample were accurately weighed in a non-hermetic sealed Tzero aluminium pan (Model 901683.901, TA instruments, New Castle, DE, USA). Then, thermograms were recorded between 5 °C and 250 °C under N_2 flux (50 ml/min) at a 10 °C/min heating rate using a Q20 Differential Scanning Calorimeter V24.7 Build 119 equipped with an RSC40 Refrigerated Cooling System (TA Instruments, New Castle, DE, USA). The instrument was previously calibrated with Indium as standard. An empty aluminium pan was used as a reference. Data analysis was performed using TA Universal Analysis 2000 software (TA Instruments, USA).

2.9. Fourier transformed infrared spectroscopy (FTIR)

Physicochemical interactions between PEOT-PBT and PLGA502 in its different polymeric blends and between indomethacin and the polymeric matrix were characterized by Fourier Transform Infrared Spectroscopy (FTIR). The KBr disks were prepared by compressing a mixture of dry samples (Indomethacin, PEOT-PBT, PLGA502, Empty-MPs and IND-loaded MPs) with KBr in an appropriate ratio (1:30–1:100). Then, transmission spectra of the samples in KBr disks were recorded in a Vertex 70v FT-MIR spectrometer (Bruker Corporation, Billerica, MA, USA) over a wavenumber range of 400–4000 cm^{-1}.

2.10. Scanning Electron Microscopy

The surface and internal morphology of the microparticles were characterized by Scanning Electron Microscopy (SEM). Before observation, whole or cross-sectioned particles were mounted on metal stubs covered with adhesive carbon tape and sputter-coated with iridium under an argon atmosphere (Q150T-S-Plus, Quorum Technologies, Laughton, UK). Afterwards, samples were observed using a ZEISS EVO LS 15 scanning electron microscope (Carl Zeiss, Jena, Germany) operated at an accelerating voltage of 15 kV and SEM micrographs were taken at appropriate magnification. In order to observe their internal morphology, microparticles were cross-sectioned after being embedded in an epoxy resin (5 Minute® Epoxy, Devcon®, Solon, OH, USA) using a modified version of a protocol previously reported [31]. Shortly, a small amount of dry sample was carefully dispersed into the epoxy resin (reagent A) until a homogeneous suspension was obtained. Subsequently, the suspension was mixed with an equal amount of hardener (reagent B) for 1 min and then allowed to dry for 1 h before cross-section the hardened pellet with a razor blade. Thin sections obtained were mounted and sputter-coated with gold/palladium (SDC 005 Sputter Coater, BAL-TEC GmbH, Schalksmühle, Germany). Then SEM micrographs were taken using a JEOL JSM-6360LV scanning electron microscope (JEOL Ltd., Tokyo, Japan) at an accelerating voltage of 15 kV and appropriate magnification.

2.11. Raman confocal microscopy

Indomethacin-loaded microspheres were analyzed by Raman confocal microscopy to assess the spatial distribution of the drug and both polymers in the microparticle structure. In brief, a small amount of dry microparticulate formulations were placed on a glass slide and observed using a WITec ALPHA300R + Raman confocal microscope equipped with a 532 nm laser and WITec Project FIVE software package (v.5.3.18, WITec Gmbh, Ulm, Germany). Before microparticles analysis, the Raman spectrum of pure indomethacin, PLGA502 and PEOT-PBT were acquired as standards.

2.12. In vitro delivery profile

In vitro release profile of indomethacin was obtained for all formulations included in the experimental design. Shortly, 20 mg of dry microparticles were suspended in 40 ml of Dulbecco's phosphate buffer saline (DPBS) supplemented with 0.02 % sodium azide into a borosilicate flask. Then, flasks were maintained at 37 °C under continuous stirring (50 r.p.m) in an orbital incubator (Unimax 1010/Inkubator 1000; Heidolph Instruments GmbH & Co., Schwabach, Germany), and 1 ml samples were withdrawn at predetermined time intervals and replaced with an equal volume of fresh medium. Experiments were performed under dark conditions to avoid indomethacin photodegradation, and *sink* conditions were maintained throughout the process. As controls, empty microparticles and a 1 μg/ml indomethacin solution were also maintained in the same conditions to assess whether degradation of the polymeric matrix or the drug's own degradation could interfere with the analytic determination of indomethacin. Finally, indomethacin concentration was determined spectrophotometrically at λ = 318 nm using an Evolution 60s UV–Vis spectrophotometer (Thermo Fisher Scientific, Waltham, MA, USA) according to the following calibration curve $\left(A_{318\,nm} = 0.0241 + 0.0166 \cdot [IND];\ R^2 = 0.9999\right)$. All experiments were performed in triplicate.

2.13. THP-1 cell culture

THP-1 human monocytic cell cultures (ATCC® TIB-202TM, American Type Culture Collection, Manassas, VA, USA) were grown in complete medium at 37 °C, under a 5 % CO_2 atmosphere with 95 % relative humidity, at a cell density between $2{\cdot}10^5$ and $8{\cdot}10^5$ cells/ml. Complete culture medium contained RPMI 1640 (Biological Industries; Cat. Nº 01-104-1A) supplemented with 10 % heat-inactivated foetal bovine serum (FBS), 25 mM D-Glucose (total concentration), 10 mM HEPES, 2 mM L-Glutamine, 1 mM Sodium Pyruvate and an antibiotic/antimycotic with a final concentration of 100 Units/ml Penicillin G, 100 μg/ml Streptomycin and 100 μg/ml Neomycin). Culture media, FBS and all supplements were purchased from Biological Industries (Cromwell, CT, USA).

THP-1 cells were differentiated into monocytic-derived macrophages by exposure to Phorbol 12-Myristate-13-Acetate (PMA) as previously reported [32,33]. In brief, cells were seeded in complete growth medium supplemented with 50 ng/ml PMA for 48 h. Afterwards, the PMA-supplemented medium was replaced by fresh medium and cultures were grown for 24 h before performing any experiments. Supplementation of culture medium with PMA was performed by adding the required volume of a 50 mg/ml PMA stock solution in DMSO to achieve a final concentration of 50 ng/ml. An equal amount of pure DMSO was assayed as a negative control.

2.14. XTT cell proliferation assays

The cytocompatibility of the IND-MPs, Blank MPs and free IND was tested by XTT cell proliferation assay. Shortly, THP-1 cells were seeded at appropriate density (15000 cells/well) in 96-well plates and differentiated into monocyte-derived macrophages as described above. A standard calibration curve for cell proliferation in the range of 117–30000 cells/well was also performed for quantification. After differentiation, test substances were added to the culture and co-incubated with cells for 24 h. Finally, 50 μl of XTT reagent was added to each well, and plates were incubated at 37 °C for 4 h before absorbance determination at λ = 450 nm. XTT reagent was freshly prepared before each experiment by mixing a 3 mg/ml phenazine methosulfate (PMS) stock solution in PBS with a 1 mg/ml XTT sodium salt solution in a phenol red-free culture medium in a 1:400 ratio.

2.15. Evaluation of phagocytic capacity

Fluorescent-labelled microparticles were fabricated following the protocol described in section 2.2. Additionally, 2.33 μg of the high lipophilic dye Coumarin 6 per gram of polymeric blend was added to the polymer solution in methylene chloride before the ultrasonic atomization process. Both fluorescence-labelled blank and indomethacin-loaded MPs were obtained.

The phagocytic activity of THP-1-derived macrophages in the presence of empty and IND-loaded MPs was investigated using a modified protocol previously reported [21]. Briefly, 50,000 THP-1 cells/well previously seeded and differentiated in black, bottom-flat 96-well plates were treated with different concentrations of Coumarin-6-loaded MPs (5–40 μg/well) and incubated for 1 or 2.5 h. Before incubation, the fluorescence signal ($\lambda_{ex}/\lambda_{em}$ = 485/520) was recorded and obtained values were set as 100 % uptake reference values. After incubation, cultures were washed in triplicate with PBS to remove non-cell-associated cells, and fluorescence was measured again in the same conditions. The percentage of uptake for each formulation after

co-incubation was calculated as the relative fluorescent intensity in relation to the 100 % uptake reference values. Eight replicates were assayed for each sample, and untreated cells were used as the negative control. For data analysis, a factorial ANOVA followed by Tukey's post hoc analysis was performed (IBM® SPSS® Statistics v 24.0, IBM Corp., Armonk, NY, USA).

Phagocytosis activity of THP-1 derived macrophages in the presence of Coumarin-6-labelled empty or indomethacin-loaded microcapsules was also evaluated by fluorescence microscopy. Cells were seeded in black, transparent bottom-flat 96 well plates as described above and then incubated at 37 °C for 2.5 h with 20 μg/well fluorescent-labelled microparticles. Then, grown medium was removed and cell cultures were washed twice and fixed for 15 min with a 3.7 % formaldehyde solution in PBS. Subsequently, the cell membrane was permeabilized for 5 min with 0.1 % Triton X-100 in PBS. Actin filaments were stained with Phalloidin-iFluor 594 to visualise the cytoskeleton according to the manufacturer protocol (Ab176757, Abcam, Cambridge, UK). Finally, the cell nucleus was stained by incubation for 5 min with a 300 nM 4′,6-Diamino-2-phenylindoledihydrochloride (DAPI) solution in PBS, followed by two washing steps with PBS. Stained cells were examined by fluorescence microscopy (Olympus IX71, Olympus Corp., Tokyo, Japan). Images from ten different areas were randomly taken for each sample (DP71 camera, Olympus Corp) with an appropriate filter for coumarin-6, DAPI and Phalloidin-iFluor 594. and then combined using Adobe Photoshop CC 2019 (Adobe Inc., San José, CA, USA). The resulting images were analyzed, and the Phagocytosis Index (PI) was expressed as the percentage of macrophages that have uptaken at least one microcapsule. All experiments were carried out in triplicate, and statistical analysis of the results was performed (IBM® SPSS® Statistics v 24.0).

2.16. TNF-α and IL-6 production

Production of some of the key inflammatory mediators involved in the pathophysiology of rheumatoid arthritis (TNF-α, IL-6) was investigated *in vitro* after exposure of THP-1 macrophages to the different blank and INF-loaded microparticulate formulations developed.

In brief, THP-1 cells were seeded in 24-well plates at appropriate density (400,000 cells/ml) and differentiated into macrophages by exposure to PMA as previously described. Once differentiated, the culture medium was replaced, and cells were pre-stimulated in the presence of LPS (2 μg/ml) for 2 h before the addition of the different treatments evaluated. Once differentiated, the medium was replaced, and the cells were stimulated with LPS (2 μg/ml) for 2 h before the treatments under investigation were added. The cells were co-incubated for 22 h in the presence of LPS, with two concentrations (200 μg/ml and 50 μg/ml) of blank MPs (F1, F4, F9) and IND-loaded MPs (F1, F4, F9), as well as with various concentrations of free IND (50–6.125 μM). Cell cultures were kept without LPS stimulation and treatment as a negative control to evaluate the basal production of the cellular products under investigation. As a positive control, the cells were stimulated with two LPS concentrations (2 μg/ml and 4 μg/ml) and grown without treatment.

The production of TNF-α and IL-6 by THP-1 cells exposed to the different experimental conditions investigated was quantified by a molecule-specific sandwich enzyme immunoassay (ELISA). For the assembly and execution of the assays, capture and detection antibody pairs for TNF-α (ab213467) and IL-6 (ab246838) were used in combination with the ELISA accessory kit (ab210905) following the protocol provided by the manufacturer (Abcam, Cambridge, United Kingdom). For quantification, each plate incorporated a calibration curve of recombinant TNF-α and IL-6 ranging between 15.6 and 1000 pg/ml for TNF-α and between 3.9 and 250 pg/ml for IL-6. All standards and samples were assayed in duplicate. Statistical analysis by ANOVA following Tuckey's test post hoc analysis was conducted.

2.17. Statistical methods

The relationships between particle size, encapsulation efficiency, and IND initial burst release with the formulation parameters assessed in the experimental design (polymeric composition and flow rate) were analyzed using a multiple quadratic regression model. The Durbin-Watson (DW) statistic test evaluated the absence of residues correlation. An ANOVA was conducted to assess the significance of the independent variables on the responses (P-value$<$0.05).

Variance analysis (ANOVA) followed by Tuckey test post-hoc analysis was performed to evaluate to assess the statistical significance of differences in ζ potential, TNF-α, and Il-6 production across all formulations. Before performing ANOVA, a Shapiro-Wilk normality test was carried out to verify that all data sets followed a normal distribution, and Levene's test assessed variance homogeneity. The Kruskal-Wallis test, followed by Bonferroni post-hoc analysis, was conducted to assess significant differences in cell compatibility and phagocytosis capacity among the formulations.

Statistical significance was defined as a p-value$<$0.05 for all statistic test carries out. Details of each analysis and results are provided in the respective methods and results sections.

3. Results and discussion

3.1. Experimental design

Experimental data obtained after the characterization of microparticles in terms of Mean Diameter (d(v,0.5)), encapsulation efficiency (E.E.), and Indomethacin's initial burst release after 1 h have been successfully fitted to a multiple regression quadratic model, and surface response graphs were constructed to assess the influence of formulation parameters over the microspheres' properties. Accordingly, to the fitted mathematical model, 93.13 % (R^2 = 0.9313; Adjusted-R^2 = 0.8969), 80.26 % (R^2 = 0.8026; Adjusted-R^2 = 0.7039) and 96.57 % (R^2 = 0.9657; Adjusted-R^2 = 0.9485) of variability on particle size (d(v,0.5)), E.E, and IND initial burst, respectively, were explained by changes in polymeric composition and contribution of both channels to the total flow rate. Additionally, the absence of correlation between the residues was confirmed by Durbin-Watson (DW) statistic (P-value$>$0.05). Statistical analysis (ANOVA) reported significant statistical relationships (P-value$<$0.05) between the independent variables studied and the responses determined. Pareto's diagrams (Fig. 2a–c, e) display the relative influence of each preparation parameter over the studied response and its significant statistical relationship. Table 2 shows the adjusted coefficients for the mathematical model (Response Variable = a•A + b•B + c•A^2+d•B^2+e•A•B + k) where A is the flow rate through the external channel and B is the percentage of PLGA502 in the polymeric blend.

3.2. Process yield and encapsulation efficiency

All formulations exhibited high process yield independently of the formulation parameters and polymeric composition. Also, high drug entrapment was achieved for all microparticulate formulations obtained, ranging between 56.20 % and 81.32 % (Table 3). As described in section 3.1, experimental data of E.E. were successfully fitted to a quadratic regression model, and surface response graphs were constructed, showing a statistically significant influence of both parameters studied over the drug entrapment achieved (Fig. 2a and b). A complex relationship between polymeric composition and E.E. was established depending on the flow rates of internal and external channels. Concisely, when the outer/inner channel flow rate ratio is high, the composition of the polymeric blend almost does not affect the E.E. Nonetheless, as this ratio decreases, the influence of the polymeric composition increases, so an inversely proportional relationship between drug entrapment and PLGA content was observed.

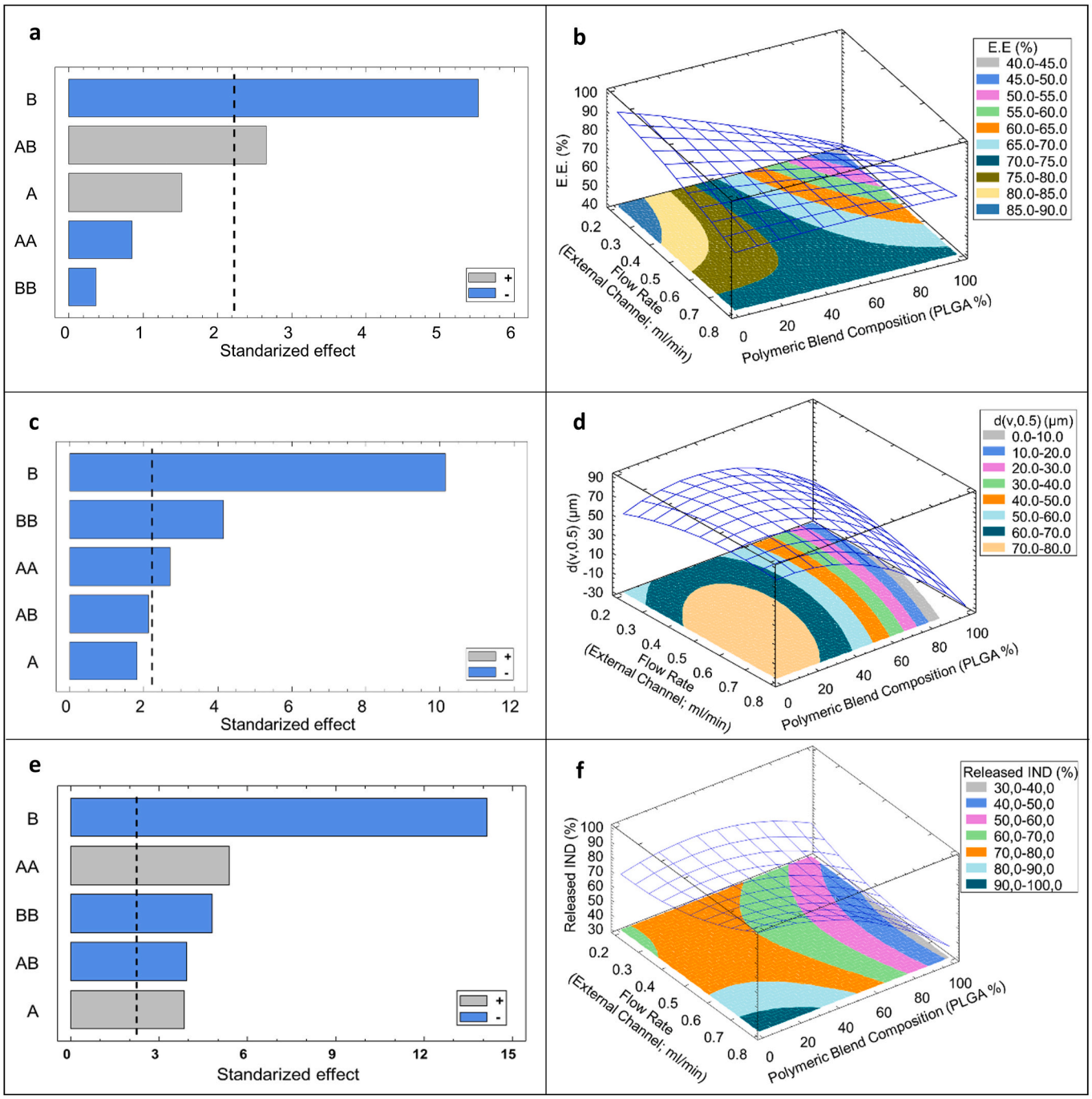

Fig. 2. Standardized Pareto's charts and surface response graphs for Encapsulation Efficiency (2a and 2b), Particle Size (2c and 2d) and IND burst release after 1 h (2e and 2f). A = External channel flow rate; B=PLGA percentage in the Polyactive®: PLGA502 polymeric blend.

Table 2
Experimental design regression coefficients.

Response variable	Regression coefficients					
	a	b	c	d	e	k
Particle size (µm)	151.8780	0.9537	−115.9210	−0.0113	−1.0290	25.6878
E.E. (%)	−9.2347	−0.5727	−22.7031	−0.0006	0.8006	92.9272
IND burst release (%)	−39.6834	0.507229	89.7186	−0.7440	−0.0051	72.5956

3.3. Particle size analysis

Particle size analysis was performed by laser diffraction, and results were expressed as volume-weighted distribution. The characteristic parameter of the distribution to describe the mean particle size of the microspheres was d(v,0.5). All microparticulate formulations included

Table 3
Process Yield, Encapsulation Efficiency and ζ potential of IND-loaded microparticles.

	Process Yield (%)	Encapsulation Efficiency (%)	ζ potential (mV)
F1	84.63 ± 1.63	72.48 ± 2.44	−12.54 ± 1.20
F2	83.12 ± 3.39	69.44 ± 1.47	−14.84 ± 2.54
F3	87.90 ± 3.54	75.22 ± 2.74	−14.05 ± 1.91
F4	88.52 ± 2.46	71.04 ± 1.46	−14.96 ± 1.17
F5	84.54 ± 4.39	81.32 ± 2.45	−15.56 ± 1.92
F6	85.16 ± 3.33	66.20 ± 1.76	−14.18 ± 1.29
F7	79.86 ± 1.90	56.29 ± 1.97	−13.23 ± 1.55
F8	86.71 ± 5.19	69.90 ± 3.47	−12.04 ± 1.14
F9	78.19 ± 1.59	66.20 ± 1.86	−13.18 ± 1.74

in the experimental design presented a monomodal and polydisperse particle size distribution, exhibiting a mean diameter ranging between 22.81 ± 0.37 μm and 82.57 ± 0.95 μm depending on formulation parameters (Table 4).

As previously stated in section 3.1, both formulation parameters (inner/outer flow rate ratio and polymeric composition) have demonstrated a significant influence over the mean particle size, explaining the 93.13 % of variability on the mean diameter of the microspheres accordingly to the fitted quadratic regression model. Furthermore, particle size was mainly determined by the polymeric blend composition, so an inversely proportional relationship was established between microspheres' mean diameter and the percentage of PLGA502 in the polymeric matrix composition.

3.4. ζ potential determination

ζ potential was measured to assess the influence of formulation parameters over the surface charge of the microspheres. All formulations showed a negative surface charge with slight differences depending on formulation parameters. (Table 3). Variance analysis (ANOVA) was performed, establishing the existence of statistically significant differences between ζ Potential values of the 9 formulations included in the experimental design (P-value = 0.000047). Further, *post-hoc* analysis by the Tuckey test revealed that significant differences (P-value<0.05) were only found between the following formulation pairs: F1-F4; F1-F5; F2-F8; F4-F8; F5-F8 and F5-F9. Before performing ANOVA, a Shapiro-Wilk normality test was carried out to verify that all data sets followed a normal distribution, and the Levene test confirmed the homogeneity of the variance. Although statistically significant differences in ζ potential values were observed, such slight differences are not expected to affect the microparticles' behavior in terms of physiological response in an *in vitro* or *in vivo* environment.

3.5. X-ray powder diffraction analysis (XRPD)

As shown in Fig. 4a, the commercial indomethacin diffraction pattern exhibited main peaks at 11.46, 16.86, 19.45, 21.65, 26.44 and 29.19° (2θ), which correspond to γ polymorph according to data previously reported [34]. Polyactive® (Fig. 3b) showed a semi-crystalline pattern with slight peaks at 16.00, 17.11, 20.64, 23.22, 24.79 and 31.16° (2θ), probably due to the presence of phase separation domains with crystalline regions in the hard PBT segment [35–37], whereas Resomer® RG 502 diffractograms (Fig. 4c) confirmed its mainly amorphous structure with single broadband centred at 19.55° (2θ) [38]. Focusing on microparticulate formulations analysis, only diffraction peaks attributable to Polyactive® were identified (Fig. 3d–i). No differences were found between empty and IND-loaded microparticles' diffractograms, suggesting that the drug is microencapsulated in an amorphous form, as confirmed by DSC and FTIR results.

3.6. Differential Scanning Calorimetry

Thermal behaviour of Indomethacin-loaded MPs, empty MPs, commercial IND, Resomer® RG502 (PLGA502) and Polyactive® was analyzed by DSC to identify the physical state of the microencapsulated drug and also, to characterize the changes in polymer properties after the microencapsulation process (Fig. 4).

DSC thermogram of pure indomethacin showed a sharp endothermic peak at 161.72 °C with a ΔH_{fusion} = 105.6 J/g characteristic of the γ polymorph melting point (T_m), in consonance with data previously reported [39]. PLGA502 thermogram exhibited a sharp endothermic peak at 48.5 °C indicative of the relaxation peak following the characteristic glass transition (T_g) of the amorphous polymer around 42-46 °C [40,41]. Polyactive® multiblock co-polymers thermal analysis is characterized by transitions of both PEOT and PBT segments due to microphase separation in a soft PEOT-rich and a hard PBT-rich region that appears as a consequence of the low compatibility of both blocks [42]. DSC thermogram of commercial Polyactive® 1000PEOT70PBT30 showed a broad endothermic band with a maximum of 160.9 °C characteristic of the PBT segment in consonance with previously reported data. Typical transitions of the PEOT segment were not detected, occurring at temperatures lower than the investigated range (T_g = −50 °C; T_m = 6 °C). Glass transition of the PBT segment was usually not detectable in copolymers with a high soft/hard segment ratio [42,43]. Three representative formulations of empty and Indomethacin-loaded formulations (F1, F4, F9) containing respectively a 50:50, 75:25 and 25:75 PLGA: PEOT-PBT ratio were also analyzed. Empty microspheres' thermograms exhibited an endothermal band between 51.2 and 51.4 °C representative of PLGA's T_g followed by a relaxation peak with lower intensity than the observed in the pure commercial polymer and another broad endothermic peak around 165 °C corresponding to PBT-segment T_m of Polyactive®. Nevertheless, in the blend's thermogram, the presence of characteristic transitions of PLGA502 and PEOT-PBT at temperatures close to those of pure materials suggests that both components are immiscible or partially miscible, which indicates that the blend is a simple mixture of both pure polymers [44]. Drug-loaded microspheres thermograms exhibited the absence of the melting peak of indomethacin (T_m = 160.9 °C), suggesting that the drug is dispersed into the polymeric matrix in an amorphous form, agreeing with X-ray diffraction results described in section 3.2.5. Characteristic transitions of PLGA and PEOT-PBT were also detected in Indomethacin-loaded microcapsules. Nonetheless, a slight shift to lower PLGA glass transition temperatures

Table 4
Characteristic parameters of IND-loaded microspheres' particle size distribution.

	d(v,0.9) (μm)	d(v,0.5) (μm)	d(v,0.1) (μm)	D [3,4] (μm)	D [2,3] (μm)	Span
F1	119.49 ± 0.30	66.29 ± 0.39	12.35 ± 0.81	69.19 ± 0.11	16.10 ± 0.14	1.616 ± 0.012
F2	106.64 ± 2.16	61.29 ± 1.12	27.70 ± 0.77	63.92 ± 1.00	16.25 ± 0.19	1.288 ± 0.024
F3	137.12 ± 3.13	82.57 ± 0.95	38.66 ± 0.22	85.08 ± 1.48	25.46 ± 0.23	1.193 ± 0.022
F4	48.32 ± 2.50	22.81 ± 0.37	4.53 ± 0.29	26.92 ± 1.88	8.48 ± 0.15	1.919 ± 0.066
F5	116.21 ± 1.27	67.55 ± 0.29	10.1 ± 0.51	69.53 ± 0.59	13.65 ± 0.10	1.568 ± 0.017
F6	70.19 ± 5.90	30.19 ± 1.01	7.63 ± 0.21	37.70 ± 4.04	9.38 ± 0.27	2.070 ± 0.118
F7	94.48 ± 3.34	45.53 ± 0.62	11.96 ± 0.07	50.78 ± 1.54	14.59 ± 0.12	1.812 ± 0.048
F8	107.85 ± 0.77	61.24 ± 0.26	9.38 ± 0.25	62.60 ± 0.33	13.38 ± 0.09	1.608 ± 0.011
F9	119.29 ± 1.54	65.41 ± 0.49	18.73 ± 0.62	68.53 ± 0.76	15.80 ± 0.17	1.537 ± 0.009

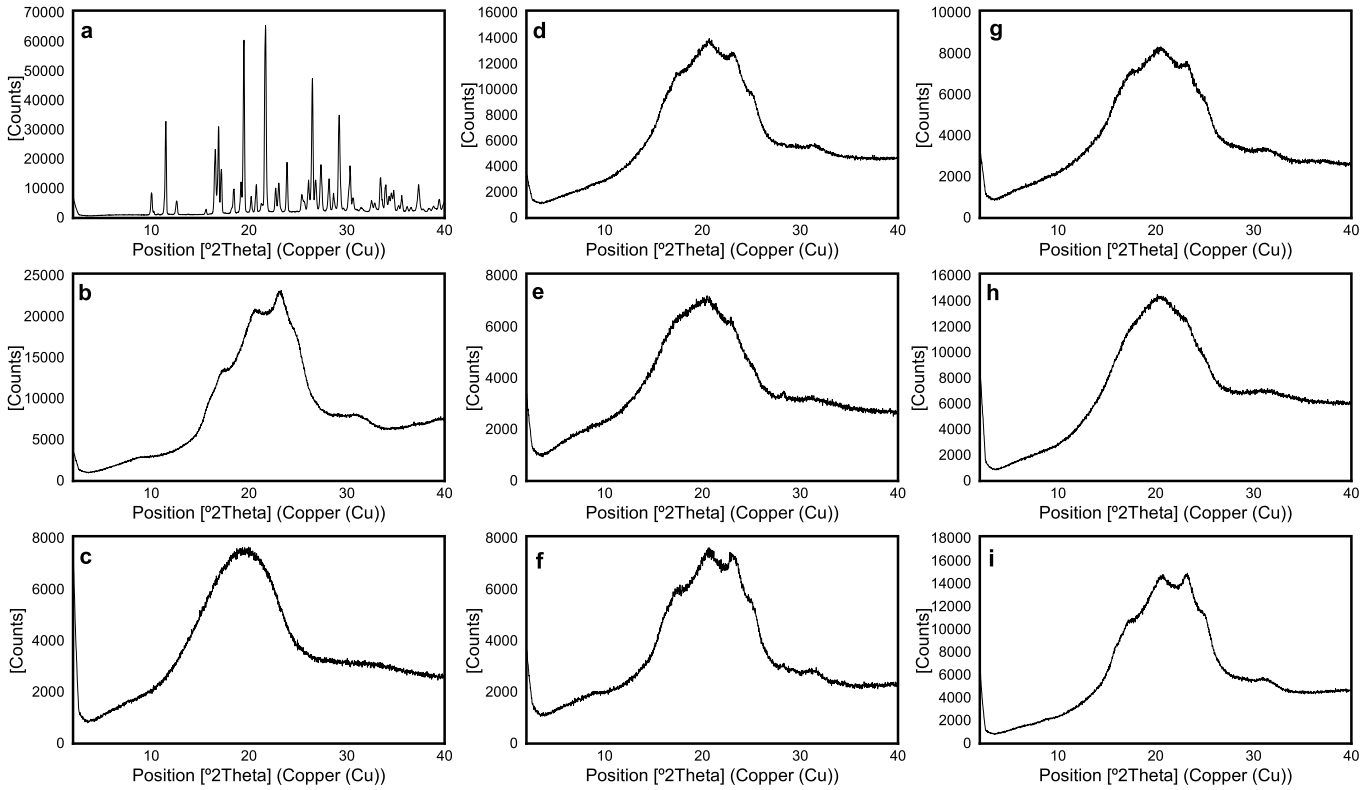

Fig. 3. X-Ray difractograms of pure Indomethacin (a), Polyactive® 1000PEOT70PBT30 (b), Resomer® RG 502 (c), Empty MPs [F1 (d), F4(e), F9 (f)] and IND-loaded MPs [F1 (g), F4 (h) and F9 (i)].

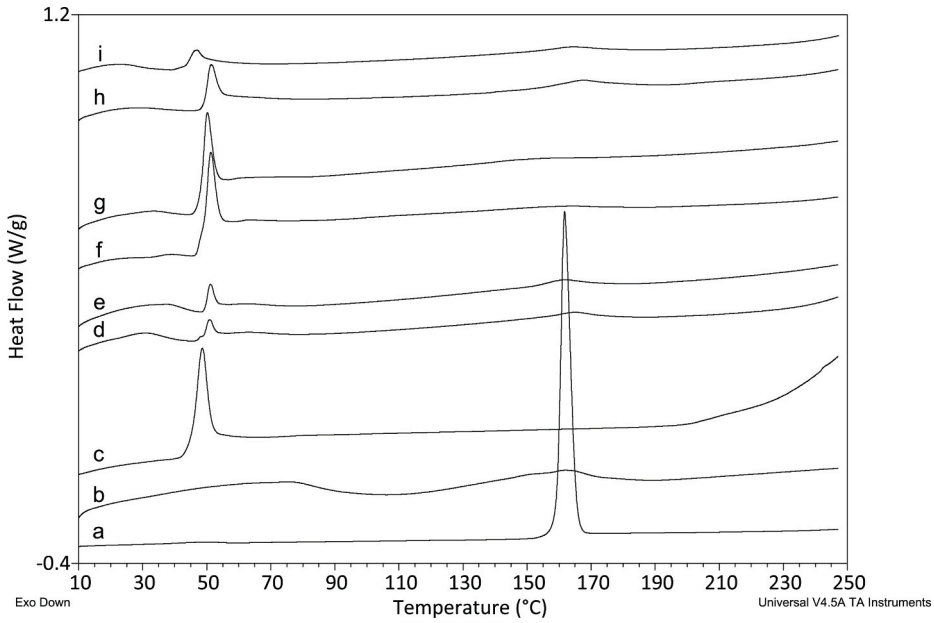

Fig. 4. DSC thermograms of γ indomethacin (a), Resomer® RG502 (b), Polyactive® 1000PEOT70PBT30 (c), Empty F9 MPs (d), Loaded F9 MPs (e), Empty F4 MPs (f), Loaded F4 MPs (g), Empty F1 MPs (h) and Loaded F1 MPs (i).

was found compared to empty MPs thermograms. Further, the shift magnitude varied depending on the formulation (F1>F4>F9). This fact can be attributed to the plasticizing effect of indomethacin on PLGA, which leads to a displacement of PLGA T_g to lower temperatures in a directly proportional relationship to IND/PLGA ratio [41,45].

3.7. Fourier transformed infrared spectroscopy (FTIR)

Resomer® RG502 spectrum (Fig. 5a) showed the most intense band at 1759.8 cm^{-1}, corresponding to characteristic ester C=O stretch, and less intense typical bans at 2999.9 cm^{-1} (CH2 bend), 1426.4 cm^{-1} (C-H deformation), 1179.1 cm^{-1} and 1094.6 cm^{-1} (C-O stretching) in consonance with already reported data [46]. Infrared spectra of

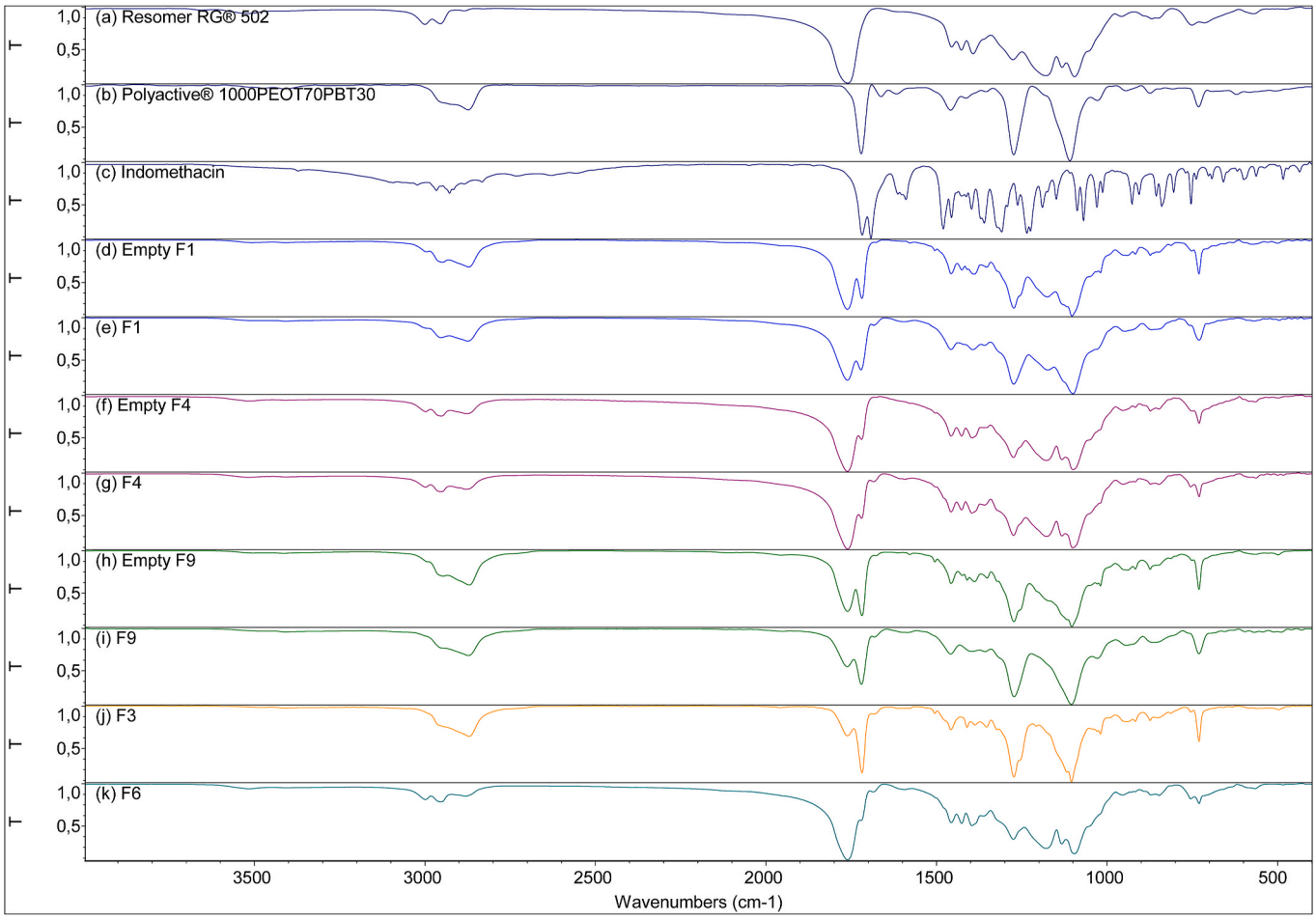

Fig. 5. FTIR spectrums of Resomer® RG502 (a), Polyactive® 1000PEOT70PBT30 (b), Indomethacin (c), Empty MPs (d,f,h) and IND-loaded MPs (e, g, i, j, k).

Polyactive® 1000PEOT70PBT30 (Fig. 5b) displayed the classic bands associated with the functional groups that are present in both segments, as previously observed for similar poly(ether/ester)s copolymers based on PEOT and PBT [47]. Broadband in the region 3000-2800 cm^{-1} related with aliphatic C-H_2 symmetric and asymmetric stretch vibrational modes was identified. Additionally, several bands related to the aromatic terephthalate units were identified, including intense peaks at 1720.1 cm^{-1} and 1272.9 cm^{-1} due to stretching vibration modes of C=O and C-O bonds of the aromatic ester and less intense peaks at 1616.8 cm^{-1} (aromatic C-C stretching), 1027.8 cm^{-1} (In-plane aromatic C-H bending) and 730.9 cm^{-1} (out of plane aromatic C-H bending). Those bands' intensity was mainly related to the copolymer's PBT segment weight fraction. Also, characteristic peaks of asymmetric and symmetric stretching vibration modes of C-O-C aliphatic ether in the soft segment were identified, respectively, at 1108.2 cm^{-1} and 872.7 cm^{-1}.

Indomethacin infrared spectrum has been reported to change depending on the crystalline or amorphous state of the drug, which confirms FTIR as a proper technique for characterizing the physical state of the drug in combination with other characterization tools like DSC or X-Ray diffraction. Concisely, a significant shift to lower wavenumbers of the characteristic band of γ polymorph at 1717 cm^{-1} was reported for amorphous indomethacin [48,49]. FTIR spectrum of pure indomethacin employed in microspheres preparation (Fig. 5c) exhibited the characteristics bands at 2927.6 cm^{-1} (O-H stretching), 1717.5 cm^{-1} (carboxylic C=O stretching), 1691.9 cm^{-1} (benzoyl C=O stretching), 1308.4 cm^{-1} (C-O stretch), 1261.6 cm^{-1} (aromatic C-O asymmetric stretching), 1086.2 cm^{-1} (aromatic C-O symmetric stretching) and 753 cm^{-1} (C-Cl stretching), agreeing with those previously reported in the literature for γ indomethacin [49,50]. These results support those obtained by DSC and X-ray diffraction as described above.

FTIR spectra of drug-free microspheres (Fig. 5d (F1), f(F4) and h (F9)) preserved the main peaks of both polymers present in the polymeric matrix, exhibiting relative peak intensity depending on the weight fraction of each one in the polymeric blend. Bands attributable to new functional groups and significant shifts were not detected, suggesting that the polymeric blend is a physical mixture of both components without a chemical reaction between both polymers. Analysis of IND-loaded microspheres (Fig. 5e (F1), g (F4), i (F9), j (F3) and k (F6)) exhibited an infrared spectrum very close to those of blank microcapsules except for the presence of small intensity peaks attributable to indomethacin. The low intensity of the drug peaks can be justified by their small proportion in the microspheres (<10 %) combined with the reduction of peak intensity reported for the amorphous state. Also, shifts in FTIR spectrum from 1713 cm^{-1} to 1708 cm^{-1} for carboxylic ester C=O band and from 1690 cm^{-1} to 1680 cm^{-1} for benzoyl carboxylic peak were reported for amorphous form compared with γ indomethacin [48,51]. Whereas carboxylic C=O stretching peak of indomethacin was not detectable due to the high intensity of carbonylic C=O band of PBT at 1720 cm^{-1}, a low-intensity peak at 1682.1 cm^{-1} was identified as the indomethacin's benzoyl C=O stretching band, shifted from 1691.9 cm^{-1} due to the amorphization of indomethacin during the microencapsulation process. Also, slight peaks or spectral changes attributable to IND were observed around 1362, 1310, 1600 and 1030 cm^{-1}.

3.8. Scanning Electron Microscopy

Microparticles' observation by SEM revealed that all formulations exhibited spherical shapes with homogeneously distributed surface

porosity. Furthermore, smaller particles with spherical or hemispherical shapes emerging from the microspheres' porous were also observed, leading to a characteristic surface morphology not previously described for microparticles made of PLGA or PEOT-PBT alone [52,53]. Although the microparticle's porosity was not analyzed, SEM micrographs revealed differences in porous surface distribution depending on polymer composition. In particular, microspheres with an equal amount of both polymers (Fig. 6a, b, h) showed a higher porous diameter with a sponge-like surface structure. Nonetheless, those formulations mainly composed of PEOT-PBT (Fig. 6c–e, i) or PLGA (Fig. 6f) exhibited smaller porous homogeneously distributed on the surface except for F4 (Fig. 6d) and F7 (Fig. 6g), which were exhibited an irregular-surface with low or no porosity.

The particle size observed agreed with results obtained by laser diffraction except for the high values reported for d(v.0,9) since no particles higher than 100 μm were observed by SEM. Those high values for 90 % undersize diameter in the volume-weighted particle size distribution can be attributed to a few microparticle aggregates, air bubbles or artefacts during analysis that can represent a high volume despite being in a small number.

To characterize the internal morphology of the microcapsules, three representative formulations composed of different ratios of PEOT-PBT: PLGA RG502 were selected: F1 (50:50), F4 (25:75), and F9 (75:25). The microparticles were successfully sectioned following the previously described protocol. However, due to the inherent limitations of the method used for sectioning the MPs and the porous nature of some formulations, it was not always possible to observe the complete cross-section of the particles.–

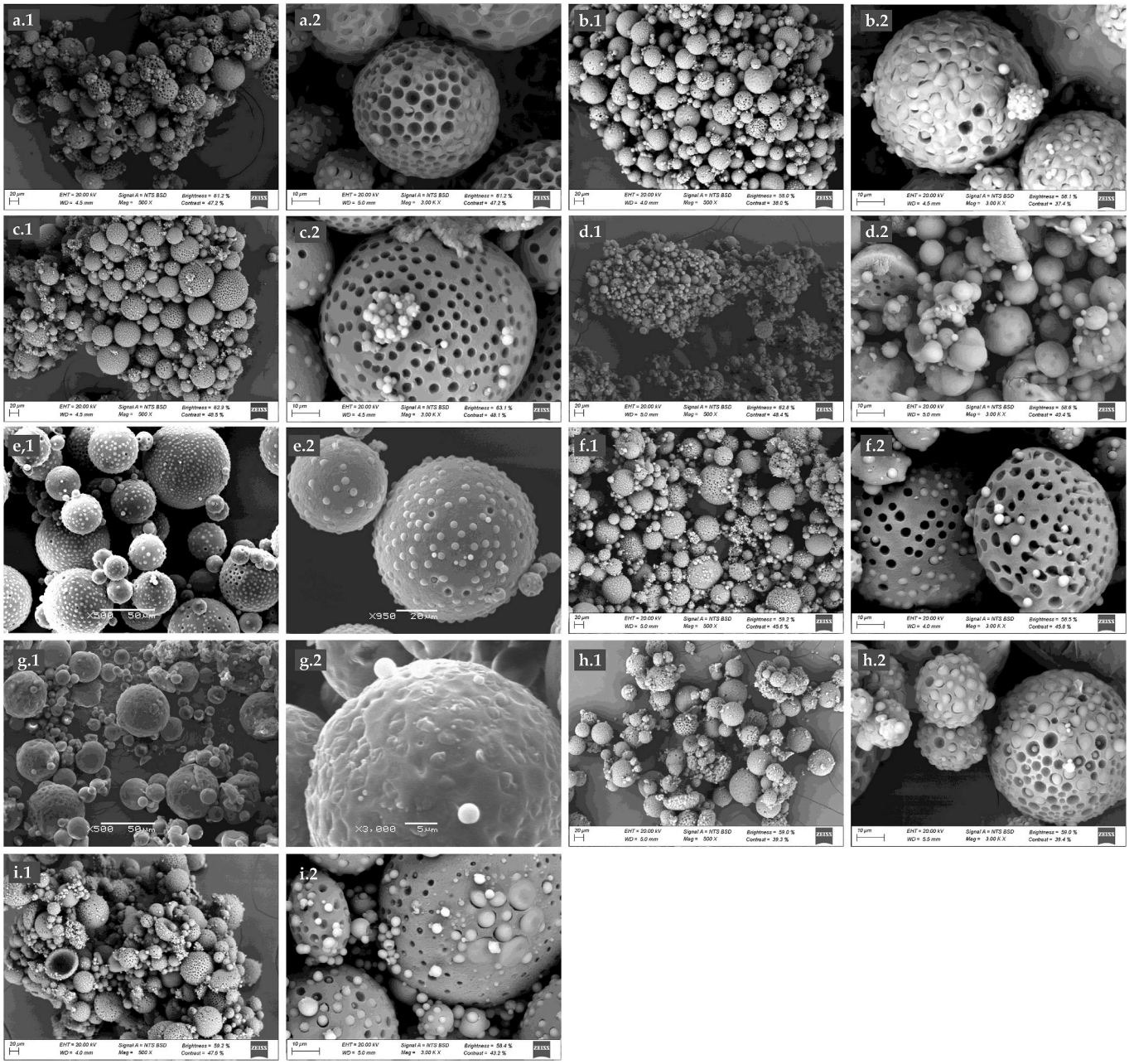

Fig. 6. Representative SEM micrographs of IND-loaded microparticles: **a.1)** F1 (*500x; SB* = 20 μm);**a.2)** F1(*3000x; SB* = 10 μm); **b.1)** F2 (*500x; SB* = 20 μm); **b.2)** F2 (*3000x; SB* = 10 μm); **c.1)** F3 (*500x; SB* = 20 μm); **c.2)** F3 (*3000x; SB* = 10 μm); **d.1)** F4 (500x; *SB* = 20 μm); **d. 2)** F4 (*3000x; SB* = 10 μm); **e.1)** F5 (*500x SB* = 50 μm); **e.2)** F5 (*3000x; SB* = 20 μm*);* **f.1)** F6 (*500x; SB* = 20 μm); **f.2)** F6 (*3000x; SB* = 10 μm); **g.1)** F7 (*500x; SB* = 10 μm*);* **g.2)** F7(*3000x; SB* = 5 μm); **h.1)** F8 (*500x; SB* = 20 μm); **h.2)** F8 (*3000x; SB* = 10 μm*);* **i.1)** F9 (*500x; SB* = 20 μm); **i.2)** F9 (*3000x; SB* = 10 μm). **SB* = *Scale Bar.*

Representative cross-sections for the different formulations investigated are displayed in Fig. 7. The cross-section of the microparticles composed of both polymers in equal proportions (Fig. 7a) showed the existence of a low-porosity core with increasing porosity in the peripheral regions, resulting in a sponge-like matrix structure not surrounded by a well-defined shell. Additionally, the presence of small particles located inside the pores with a peripheral distribution was observed. This type of internal structure had not been previously observed in PEOT-PBT or PLGA microparticles, as well as the distinctive external surface where small particles appear to emerge from within the microcapsules through the surface pores.

Formulation F4, with a high content of PLGA502 (75 %), was characterized by MPs with a non-porous matrix structure (Fig. 7b1). However, some MPs with a thick non-porous outer layer surrounding a small cavity with small particles located on its inner surface were observed. These findings are consistent with the absence of surface porosity observed for this formulation (Fig. 6d), as well as with the results from confocal Raman microscopy, which suggested the presence of a more homogeneous polymeric matrix with PLGA and PEOT-PBT enriched domains without a defined spatial distribution (Fig. 8c). Finally, MPs mainly composed of PEOT-PBT (F9) exhibited an internal structure characterized by pores with small spherical particles inside them (Fig. 7c1 and 7c.2). In contrast with the structure observed for F1, these small particles were located in the central region of the MPs rather than on the external surface. In some particles, a higher density was observed at the outer edge, simulating a partially porous covering enveloping the porous matrix structure. The observed morphology confirms the confocal Raman data, indicating that randomly positioned small particles in F9 MPs correspond to PLGA-rich regions (Fig. 8f).

3.9. Raman confocal microscopy

Raman spectrums of empty and IND-loaded MPs in a cross-section plane were acquired using a confocal Raman microscopy equipped with a 532 nm laser. Spatial distribution of the component was achieved by filtering the MPs spectrum by a characteristic RAMAN band of each component, and then images were created. For better comprehension of results, images displaying the spatial distribution of each component into the MCs were combined to create a unique image where the areas with a higher content of each component were displayed according to a colour scale.

Empty and IND-loaded MPs analysis showed a heterogeneous distribution of both constituents of the polymeric blend in the microspheres. Concisely, empty F1 MPs (Fig. 8a), which contain an equal amount of both components, showed a more homogeneous distribution of PEOT-PBT over the polymeric matrix, whereas spot areas with a high content in PLGA were observed especially near the MPs borders. Similar results were obtained for all IND-loaded MPs containing more than 50 % PEOT-PBT (Fig. 8d–f). The compassion of those results with SEM micrographs suggested the existence of a main porous structure with a high content of Polyactive® that coexisted with spot areas mainly composed of PLGA, which seemed to correspond to the smaller particles observed emerging from the MPs' porous. Nevertheless, MPs with a higher PLGA502 content showed main PLGA structures with PEOT-PBT regions mainly localized in the non-peripherical regions where IND was also found (Fig. 8c–e).

Regarding drug localization within the MPs, the IND distribution pattern was related to its presence in PEOT-PBT-rich domains. To clear visualization, the spatial distribution of the three components in F1 was displayed separately (Fig. 8b), clearly showing the correlation between PEOT-PBT (Fig. 8b2) and IND (Fig. 8b3) localization patterns. Those results agreed with the high drug entrapment exhibited by formulations with a high PEOT-PBT content, even when a small outer/inner channel flow ratio was employed. This fact suggested a high affinity of IND for hydrophobic domains of PEOT-PBT, which contrast with the high *in vitro* drug delivery rates found for MPs with a higher content in PEOT-PBT (Fig. 9). Although several authors have previously characterized the behaviour of PEOT-PBT copolymers in microencapsulation of proteins and small hydrophilic drugs [21,54,55], further research should be performed to elucidate its interactions with high hydrophobic drugs like indomethacin.

Analysis of MPs with a 75:25 PLGA: PEOT-PBT ratio (Fig. 8c–e) revealed the encapsulation of IND in non-peripheric PEOT-PBT domains. Also, a PLGA-rich continuous shell surrounding a PEOT-PBT core containing IND and PLGA spots was observed when a small outer/inner channel flow rate ratio was used (Fig. 8e), which agrees, from a morphological point of view, with the non-porous surface observed by SEM for this formulation (Fig. 6g). Nevertheless, MPs with a 25:75 PLGA:PEOT-PBT ratio (Fig. 8d–f) exhibited an IND distribution in the interface between both polymeric domains, being more evident in F5, prepared with a small external/internal channel flow rate ratio (Fig. 8d). IND peripherical distribution or interfacial areas easily accessible to water could contribute to the greater burst release observed *in vitro* for those formulations compared to those with higher PLGA content. Concisely, the continuous PLGA shell observed in F7 by Raman confocal microscopy (9e), and SEM (Fig. 6g) may explain the lower burst release

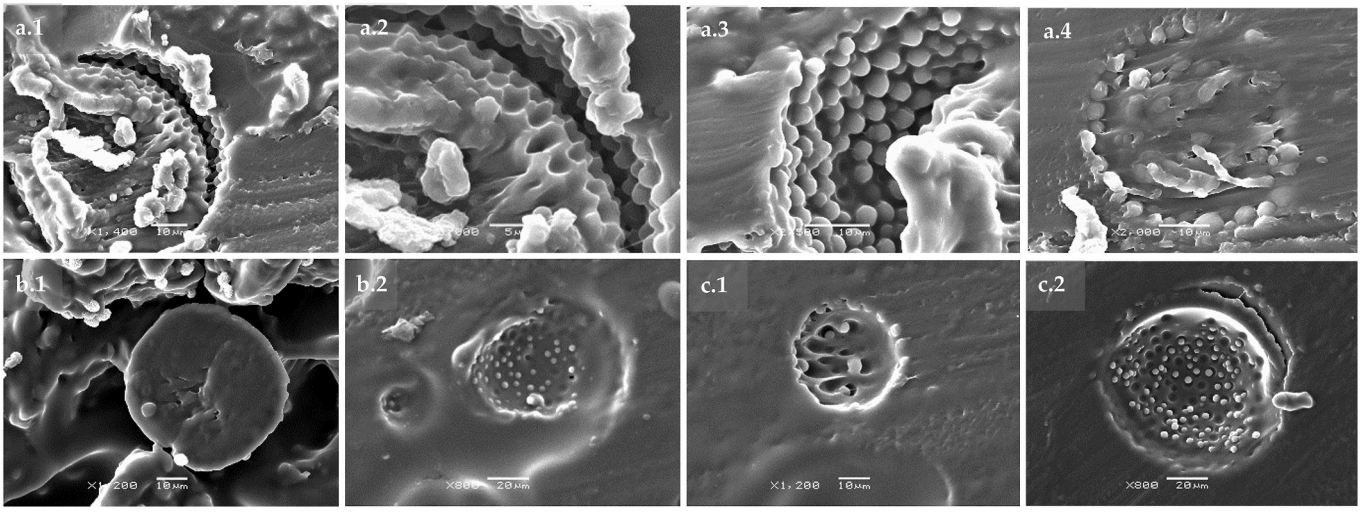

Fig. 7. Representative micrographs of the cross-sections of IND-loaded microparticles: **a.1) F1** (SB = 10 μm); **a.2) F1** (SB = 5 μm); **a.3) F1** (SB = 10 μm); **a.4) F1** (SB = 10 μm); **b.1) F4** (SB = 10 μm); **b.2) F4** (SB = 20 μm); **c.1) F9** (SB = 10 μm) and **c.2) F9** (SB = 20 μm).

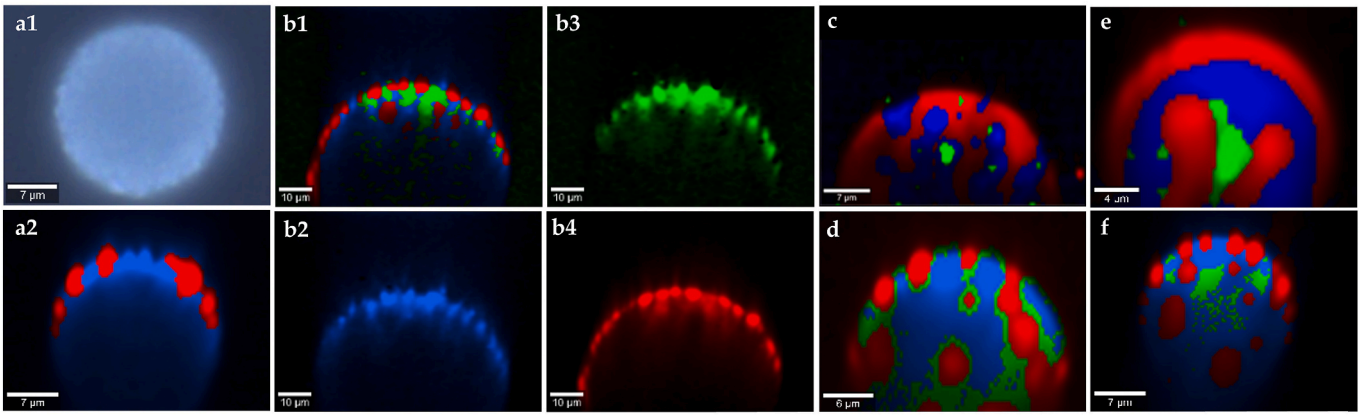

Fig. 8. Optical confocal image of empty F1 MP (a1) and Color-coded Raman images of Empty F1 (a2) and IND-loaded F1 (b1-4), F4 (c), F5 (d), F7 (e) and F9 (f). Red = PLGA502; Blue = PEOT-PBT; Green = Indomethacin. (For interpretation of the references to colour in this figure legend, the reader is referred to the Web version of this article.)

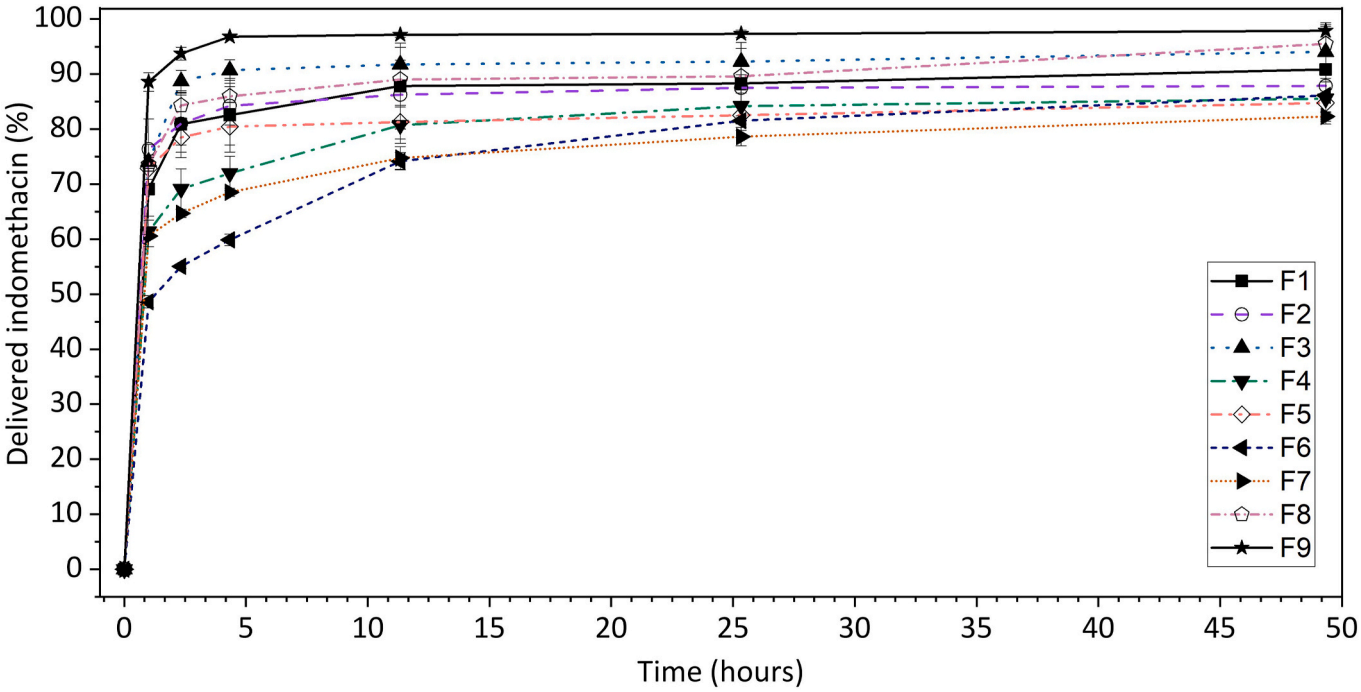

Fig. 9. *In vitro* release profile of IND at pH 7.4 and 37 °C under sink conditions. All experiments were performed in triplicate. Released IND was expressed as percentage of the total IND loading for each formulation.

and drug delivery rate exhibited for this formulation *in vitro*. Finally, we can conclude that although further analysis is needed to understand the physicochemical interactions and the underlying mechanisms for the observed morphology, the presence of distinct regions with a predominant content of one polymer supports the DSC results, suggesting limited miscibility between both components of the polymer matrix.

3.10. In vitro delivery profile

After an initial burst of loaded-IND ranging between 48.6 % and 88.6 % in the first hour, depending on the formulation parameters (F6<F7<F4<F1<F5<F8<F3<F2<F9), an IND sustained release was achieved once a plateau was reached (Fig. 9). After 50 h, the delivery assay was concluded, with 82.3 %–97.9 % of the total encapsulated IND delivered, depending on the formulation. Experimental data of the percentage of drug delivered in the first hour were successfully fitted to a mathematical quadratic model to assess the impact of formulation parameters over the initial burst release, and a surface-response graph was also constructed (Fig. 2e and f).

A significant influence of polymeric composition over the magnitude of the initial burst was observed, so an inverse proportional relationship was established between the percentage of PLGA in the polymeric blend and the IND initial burst. The analysis of the statistically significant results concluded that an increment in the outer/inner channel flow rate ratio leads to a rise in the drug's initial burst. However, a more complex relationship between both parameters can be observed in Fig. 2e. In particular, when the polymeric matrix was rich in PEOT-PBT, an increase in the external channel flow rate boosted the initial burst effect. Nevertheless, the inverse effect was observed when a polymeric blend with a high content of PLGA was used.

3.11. Cell biocompatibility

XTT viability assay results are displayed in Fig. 10, showing high cell

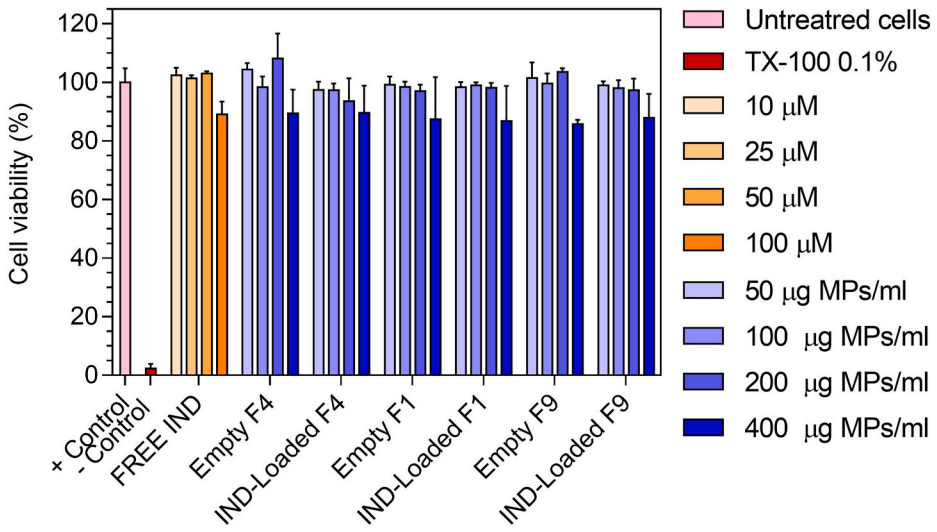

Fig. 10. Percentage of THP-1-derived macrophages viability rated obtained by XTT assay upon cell incubation with free IND, empty and IND-loaded microparticles for 24 h. All experiments were performed in triplicate.

compatibility of the microparticles with viability rates near 100 % for all formulations assayed. Statistical analysis results performed by Kruskal-Wallis non-parametric test revealed significant differences in cell survival (p-value = 0.00017) between untreated cells and cells co-incubated with empty or IND-loaded microparticles for 24 h. Nonetheless, post-hoc analysis by Bonferroni showed that statistical differences (p-value<0.05) in cell viability were only found between untreated and treated cells at the highest dose (400 μg/ml) of microparticles. Moreover, statistically significant differences in cell survival were not established between untreated cells and those incubated with the three formulations when applied at doses equal to or lower than 200 μg MP/ml. The absence of indomethacin toxicity to THP-1 at the concentrations used in cell culture assays was also verified. Although a slightly lower viability rate (89.1 ± 4.4 %) was observed for the maximum IND concentration assayed, no statistically significant differences were found by the Kruskal-Wallis test (P-value = 0.062) over the concentration range studied (10–100 μM).

According to the statistical analysis results, the presence of IND in the microparticles has been demonstrated not to affect cell viability when compared with the same drug-free formulation in the same conditions (p-value>0.05). These results agreed with the absence of IND toxicity in this concentration range, considering that theoretical drug concentration achieved after the complete delivery of micro-encapsulated IND for the highest MPs dose assayed was below 100 μM (theoretical loading = 10 μg IND/100 μg MP), even though the final concentration of IND in the culture medium depends on multiple factors and is not entirely known. Reduction in viability rates (85.5–88.7 %) obtained for THP-1 macrophages treated with 400 μg/ml of blank or IND-loaded MPS seems to be related rather to the presence of high microparticle's density in the culture well than with the toxicity of the polymeric material. Furthermore, the high biocompatibility of both polymers in the composition of the MPs has been extensively reported. Moreover, cellular response changes and cell viability reduction were previously reported by several authors when high concentrations of MPs were used [56], probably due to the mechanical effect of the high amount of MPs on the culture well over cell monolayer. According to obtained results, a non-toxic concentration range was selected for further *in vitro* characterization assays in THP-derived macrophages.

3.12. Phagocytic activity

Phagocytosis activity of THP-derived macrophages upon F1, F4 and F9 microparticulate formulations was assessed using a fluorescence-based quantitative assay and UV optical microscopy. All experiments were performed in the absence of LPS stimulation. As can be seen in Fig. 11a quantitative results of the assay have been shown that the microparticles were highly phagocyted by THP-1 cells in a significant time-dependent and dose-dependent manner. Also, significant differences were found depending on the microparticulate formulation since a correlation between PLGA content in the MPs, and phagocytosis percentage could be established. This effect was, probably due to the strong influence of polymeric blend composition over particle size distribution, which represents a critical factor in the phagocytosis process as previously reported by several authors [57,58]. As shown in Fig. 11a, F4 exhibited the highest percentage of MPs phagocyted followed by F1 and F9, with the independence of the incubation time or the dose assayed. When incubation time increased from 1 to 2.5 h, a more significant boost in F4 phagocytosis percentage was observed compared to those observed for F1 and F9. A decrease in incubation time influence was also observed when tested lower concentrations of MPs. Those results can probably be explained by the significant minor diameter of F4 MPs. As a matter of fact, quicker and more extensive internalization was previously reported for smaller particles, exhibiting an inverse relationship between particle diameter and the average number of MPs uptaken per cell [58].

Furthermore, high internalization of the MPs by the macrophages was stated by UV optical microscopy as shown in representative micrographs (Fig. 11b–d), where intracellular spherical microspheres could be observed. Phagocytosis index (PI), which represents the percentage of cells that phagocyted at least one microparticle, was higher than 95 % for the three formulations assayed. In summary, both assays performed demonstrated that all microparticulate formulations were extensively internalized by THP-1 cells, effectively targeting macrophages and allowing intracellular delivery of IND.

Phagocytosis has been reported to depend on particle size, shape, surface charge and hydrophobicity [59]. Regarding particle size, although microparticles with a diameter lower than 10 μm are often considered adequate for phagocytosis, a general cutoff can not be established due to the complexity of factors involved in the phagocytic process [58,59]. In fact, the internalization of microparticles, even with greater diameters than the cells, has been previously reported [60]. Macrophages have been demonstrated to play a central role in the physiopathology of RA as the main amplifiers of inflammation, making macrophage targeting an attractive approach to rheumatoid arthritis treatment [61,62]. Due to the polydisperse distribution of the IND-loaded MPs obtained and their average mean diameter (22.8–66.3

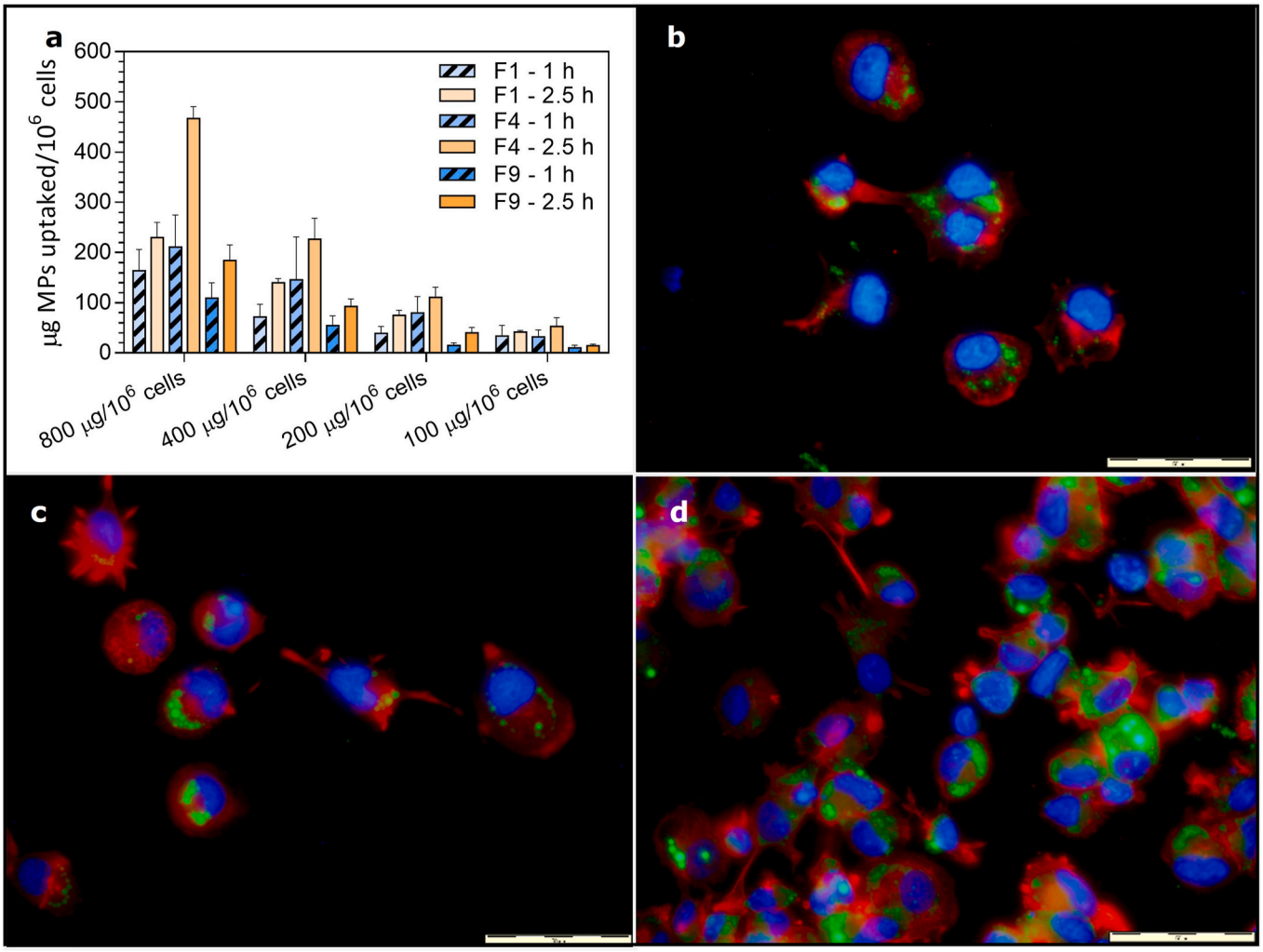

Fig. 11. Micrograms of microparticles phagocyted by THP-1 macrophages after incubation for 1 or 2.5 h (a). UV micrographs of F1 (b), F4 (c) and F9 (d) fluorescence-labelled microparticles phagocyted by THP-1 macrophages. MPs are displayed in green, cell nucleus in blue and actin filaments in red. Scale Bar = 50 μm. (For interpretation of the references to colour in this figure legend, the reader is referred to the Web version of this article.)

μm), only a formulation fraction can be potentially internalized by the macrophages, leading to an intracellular delivery of IND. This strategy would allow a specific targeting to phagocytic cells and an extracellular delivery in the articular space. Accordingly, to well-known phagocytosis mechanisms, the particle engulfment involves a membrane extension to envelop the target to form a phagosome containing the phagocyted IND-loaded MP. After phagosome maturation, it can fuse with lysosomes, leading to a highly acidic environment and several degradative enzymes [59]. Despite *in vitro* delivery assays showing a rapid IND delivery rate, the results obtained under sink conditions at physiological pH were not completely predictable in intracellular IND delivery from phagocyted MPs. Although the IND intracellular delivery profile cannot be elucidated, several factors, such as small intracellular volume and lower drug solubility in a highly acidic environment, point to a slower IND delivery, whereas enhanced polymeric degradation can stimulate IND release. Also, IND stability upon internalization should be further investigated, even though its high stability at acidic pH values was already reported [63,64]. Delivered lipophilic IND could easily diffuse from the phagolysosomal membrane and reach the cytoplasm. COX-2 induction and overexpression in inflamed joint tissues have been reported in RA, which causes an increase in prostaglandin levels and exacerbates the inflammatory reaction. Moreover, synovial macrophages were reported as the main producer of inducible COX-2 in RA, which is mainly localized in the cytoplasm [65,66]. Therefore, microparticulate formulations seem to be a promising approach to intracellular delivery of IND, inhibiting COX activity and achieving an anti-inflammatory effect using low doses while improving the systemic toxicity profile.

3.13. Antiinflammatory activity in vitro

Indomethacin exhibits high efficacy in the treatment of rheumatic diseases like RA. As an AINE, it exerts its anti-inflammatory activity by blocking prostaglandins' production by COX [1]. Nonetheless, there is no consensus about its effect on the production of TNF-α, IL-6 and other key pro-inflammatory mediators in RA [67–69]. In this work, the effect of free and microencapsulated IND (F1, F4, F9) over the production of TNF-α and IL-6 was evaluated *in vitro* in LPS-stimulated THP-1-derived macrophages.

Quantification of TNF-α and IL-6 concentration in the cell culture supernatants was performed by ELISA according to the respective calibration curves previously obtained using recombinant TNF-α and IL-6 standards. The relationship between the decimal logarithm of TNF-α concentration and absorbance (λ = 450 nm) resulted in an asymmetric sigmoidal curve that fitted a five-parameter logistic regression model (R^2 = 0.9999; Adj-R2 = 0.9995). The relationship between IL-6 concentration and absorbance fitted a second-degree polynomial model (R2 = 0.9999; Adj-R^2 = 0.9999).

Treatment of THP-1 macrophages with microencapsulated IND

reduced TNF-α production compared to the positive LPS control (2 μg/ml). A statistically significant reduction was reached after treatment with 200 μg of IND-MPs from formulations F1 and F4, whereas statistical significance was not reached for formulation F9 at the same dose. That fact could be attributed to the lower encapsulation efficiency of F9 compared to F1 and F4 (Fig. 12A). Moreover, treating macrophages with all IND-loaded microparticulate formulations investigated resulted in a statistically significant dose-dependent reduction in IL-6 levels. Specifically, incubating macrophages with a 200 μg/ml dose of MPs from F1, F4, and F9 led to a 74 %, 68 %, and 54 % reduction in IL-6 production, respectively, demonstrating their high *in vitro* anti-inflammatory capacity (Fig. 12).

Production of TNF-α and IL-6 was also investigated in response to free IND (12.5–50 μM). A statistically significant reduction in TNF-α synthesis was only achieved after cell incubation with the highest IND concentration assayed (50 μM). If we keep in mind that this free-IND concentration is higher than the maximum theoretical concentration that could be achieved after complete release of IND entrapped in 200 μg of MPs (Table 5), in combination with the higher decrease of TNF-α and IL-6 levels achieved after cell treatment with lower doses of microencapsulated IND (F1, F4), its reasonable to conclude that microparticulate IND formulations exhibiting a stronger *in vitro* anti-inflammatory effect in comparison to free drug. This may be hypothetically explained by the delivery of IND to the cytosol of macrophages after the internalization of IND-loaded microparticles, causing COX inhibition primarily in the cytoplasm and thereby minimizing the activation of the inflammatory cascade, as discussed in section 3.12.As a control, it should be noted that cell treatment with drug-free formulations did not lead to a statistically significant increase in the production

Table 5
Free IND theoretical concentration that would be achieved after the complete release of microencapsulated IND for both MP concentrations assayed (200 y 50 μg MP/ml).

Formulation	IND Concentration (μM)	
	200 μg MP/ml	50 μg MP/ml
F1	40.5 μM	10.1 μM
F4	39.7 μM	9.9 μM
F9	37.0 μM	9.0 μM

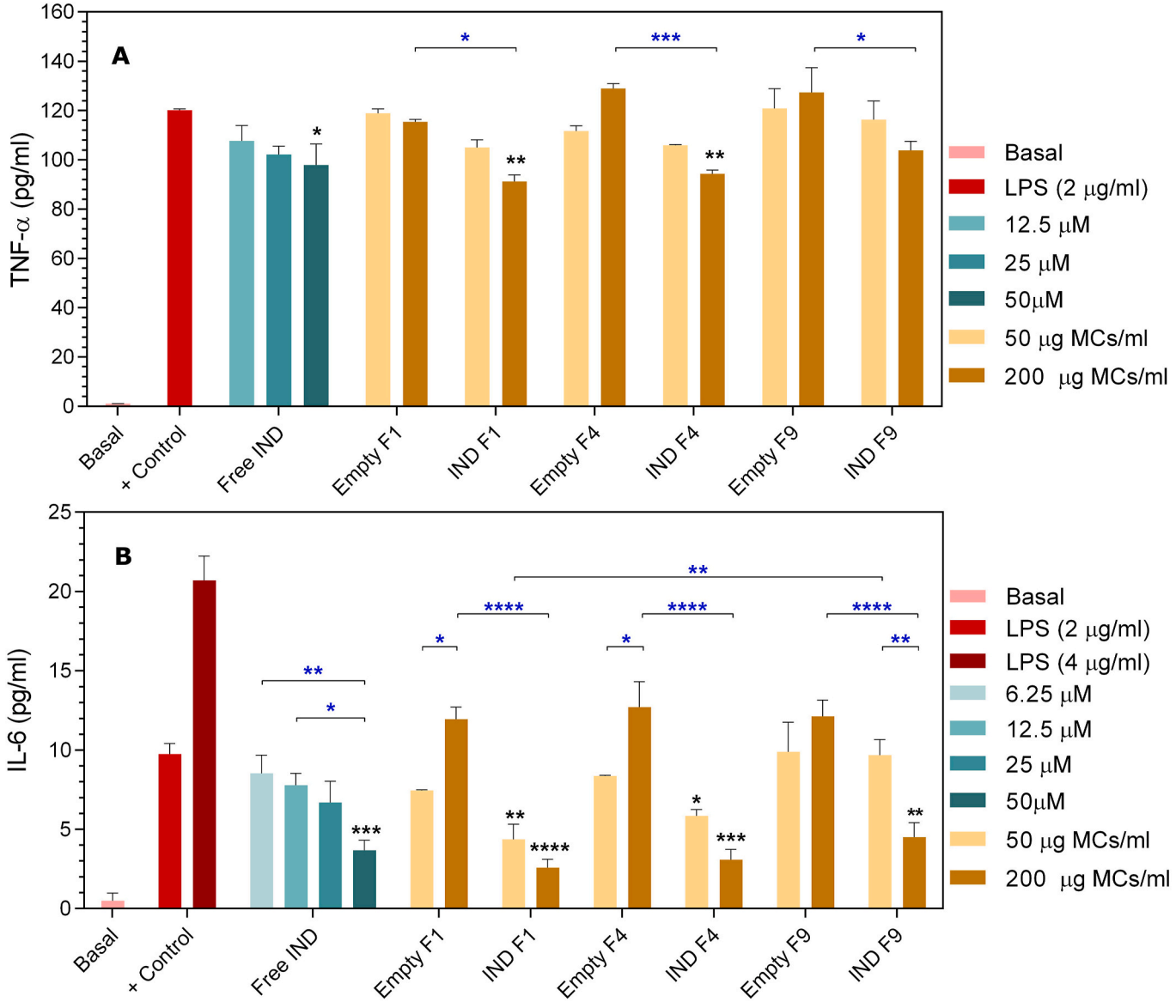

Fig. 12. TNF-α (A) and IL-6 (B) production by LPS-stimulated THP-1-derived macrophages after exposure to empty MPs, IND-loaded MPs, and free IND. All experiments were performed in triplicate. *(p ≤ 0.05); **(p ≤ 0.01); ***(p ≤ 0.001); ****(p ≤ 0.0001).

of TNF-α and IL-6 (Fig. 12), confirming that polymeric microparticles did not exhibit an inherent anti-inflammatory or pro-inflammatory effect on macrophages. Despite the absence of statistically significant differences from the LPS control, both mediators' production was slightly higher in response to the maximum investigated dose of blank MPs.

There is no consensus regarding the effect of IND and other NSAIDs on the production of TNF-α and IL-6. In contrast with our results, Spatafora et al. investigated the effect of IND on TNF-α production by primary human monocytes stimulated with LPS, concluding that IND stimulated the release of TNF-α, probably as a result of its ability to inhibit the endogenous production of prostaglandin E2 [69]. Likewise, Page et al. evaluated the impact of various NSAIDs on TNF-α and IL-6 production in LPS-stimulated human monocytes and synovial membrane primary cultures from RA patients, demonstrating the ability of NSAIDs to induce TNF-α production but not other cytokines such as IL-6 or IL-1 [68].

However, supporting our *in vitro* results, several studies have shown the opposite effect, with a reduction in TNF-α and IL-6 in response to IND treatment. Specifically, intra-articular treatment with nanoencapsulated IND resulted in a statistically significant decrease in the production of TNF-α and IL-6 in an *in vivo* model of collagen-induced arthritis in rats, while the administration of the free drug did not lead to a significant decrease in the levels of both mediators (Yin et al., 2020a). Other authors observed in a rat arthritis model a reduction in the production of TNF-α and an improvement in the inflammatory level after treatment with free and micelle-encapsulated IND [67]. Furthermore, the oral treatment of an *in vivo* RA model with IND nanocapsules reduced TNF-α and IL-6 levels [23].

According to the results, microparticulate formulations of IND show promising potential in treating RA through intra-articular administration. Data obtained *in vitro* demonstrated their suppressive capacity on producing IL-6 and TNF-α, two pivotal inflammatory mediators in RA.

4. Conclusions

Nine different formulations of Indomethacin-loaded polymeric microparticles made of PEOT-PBT and PLGA502 at different ratios were successfully developed by coaxial ultrasonic atomization according to a central composite experimental design, exhibiting high process yield (78.2–88.5 %). The microparticulate formulations were characterized in terms of particle size, encapsulation efficiency and *in vitro* delivery of IND and achieved data were analyzed by surface-response methodology to assess how the inner/outer flow rate and polymeric composition influence the features of the microparticles.

Spherical polydisperse microparticle formulations with a mean diameter of 22.8 and 82.6 μm were obtained, demonstrating an inverse relationship between particle size and the percentage of PLGA502 in the polymeric matrix. Regarding encapsulation efficiency, our results evidenced the high efficacy of ultrasonic atomization encapsulating indomethacin, establishing a complex relationship between formulation parameters and encapsulation efficiency (56.2 and 81.32 %). All formulations showed suitable *in vitro* release profiles to achieve a sustained release of indomethacin for 50 h, even though all formulations exhibited a significant burst effect of magnitude directly proportional to the PEOT-PBT content on the polymeric matrix.

The extensive physicochemical characterization confirmed that the encapsulation process did not degrade or modify the polymers' properties. Moreover, the heterogeneous distribution of both polymers in the microparticles combined with morphology and DSC results suggested low PEOT-PBT and PLGA502 miscibility. Concerning the spatial distribution of indomethacin within the polymeric matrix, RAMAN confocal microscopy analysis concluded that the drug was mainly located in the PEOT-PBT-rich domains and the interface between the regions rich in PEOT-PBT and PLGA-rich domains.

The biocompatibility of IND-loaded microparticles was confirmed *in vitro* in cell cultures of THP-1 macrophages, achieving viability rates near 100 %. Further, the macrophages extensively phagocyted microparticles in a time and dose-dependent manner. Indomethacin-loaded microparticles demonstrated their anti-inflammatory activity *in vitro*, leading to a statistically significant reduction in the production of IL-6 and TNF-α by LPS-stimulated THP-1 macrophages compared to the LPS positive control. It should be noted that a higher magnitude of the anti-inflammatory effect was observed in response to microencapsulated indomethacin compared to equivalent doses of free drug.

In conclusion, ultrasonic atomization is revealed to be a suitable technology for preparing IND-loaded microparticles with suitable properties for the intra-articular delivery of indomethacin, targeting macrophages and achieving effective retention into the joint. Also, this technique allows us to modulate microparticles' features depending on the formulation parameters. Those findings, in combination with the high anti-inflammatory activity observed *in vitro,* established IND-loaded microparticles as a promising approach for the local treatment of rheumatoid arthritis. Despite these promising results, a further preclinical investigation should be performed *in vivo* to confirm these formulations' therapeutical potential and establish the therapeutical doses in the intra-articular space.

Funding

Iván Lamela-Gómez is grateful to "Axudas á etapa predoutoral da Xunta de Galicia, cofinanciadas polo programa operativo FSE Galicia 2014-2020" predoctoral grant program. Consellería de Cultura, Educación e ordenación universitaria, Xunta de Galicia, Spain. This research was partially funded by Consellería de Cultura, Educación e ordenación universitaria, Xunta de Galicia, Spain. Axudas para a consolidación e estructuración de unidades de investigación competitivas Modalidad A: Grupos de Referencia Competitiva (ED341C 2017/13).

CRediT authorship contribution statement

Iván Lamela-Gómez: Writing – review & editing, Writing – original draft, Visualization, Methodology, Investigation, Formal analysis, Conceptualization. **Asteria Luzardo-Álvarez:** Writing – review & editing, Writing – original draft, Supervision, Resources, Methodology, Funding acquisition, Conceptualization.

Declaration of competing interest

The authors declare that they have no known competing financial interests or personal relationships that could have appeared to influence the work reported in this paper.

Data availability

Data will be made available on request.

References

[1] S. Lucas, The pharmacology of indomethacin, Headache J. Head Face Pain 56 (2016) 436–446, https://doi.org/10.1111/head.12769.
[2] S. Nalamachu, R. Wortmann, Role of indomethacin in acute pain and inflammation management: a review of the literature, Postgrad. Med. J. 126 (2014) 92–97, https://doi.org/10.3810/pgm.2014.07.2787.
[3] M. Alkholief, M.A. Kalam, M.K. Anwer, A. Alshamsan, Effect of solvents, stabilizers and the concentration of stabilizers on the physical properties of poly(d,l-lactide-co-glycolide) nanoparticles: encapsulation, in vitro release of indomethacin and cytotoxicity against HepG2-Cell, Pharmaceutics 14 (2022), https://doi.org/10.3390/pharmaceutics14040870.
[4] Z. Norouzi, M. Abdouss, Electrospun nanofibers using β-cyclodextrin grafted chitosan macromolecules loaded with indomethacin as an innovative drug delivery system, Int. J. Biol. Macromol. 233 (2023) 123518, https://doi.org/10.1016/j.ijbiomac.2023.123518.
[5] Z. Xie, L. Wang, J. Chen, Z. Zheng, S. Srinual, A. Guo, R. Sun, M. Hu, Reduction of systemic exposure and side effects by intra-articular injection of anti-inflammatory

agents for osteoarthritis: what is the safer strategy? J. Drug Target. 31 (2023) 596–611, 10.1080/1061186X.2023.2220083.
[6] H. Ping-Hsuan, W. Olivia, G. Claudia, M. Emma, B.M. Iain, S. Stefan, Economic burden of rheumatoid arthritis: a systematic review of literature in biologic era, Ann. Rheum. Dis. 79 (2020) 771, https://doi.org/10.1136/annrheumdis-2019-216243.
[7] C. Delpech, F.-X. Laborne, P. Hilliquin, Comparison of biological agent monotherapy and associations including disease-modifying antirheumatic drugs for rheumatoid arthritis: literature review and meta-analysis of randomized trials, J. Clin. Med. 12 (2023) 286, https://doi.org/10.3390/jcm12010286.
[8] D. Aletaha, J.S. Smolen, Diagnosis and management of rheumatoid arthritis: a review, JAMA 320 (2018) 1360–1372, https://doi.org/10.1001/jama.2018.13103.
[9] N. Butoescu, O. Jordan, E. Doelker, Intra-articular drug delivery systems for the treatment of rheumatic diseases: a review of the factors influencing their performance, Eur. J. Pharm. Biopharm. 73 (2009) 205–218, https://doi.org/10.1016/j.ejpb.2009.06.009.
[10] L. Fraenkel, J.M. Bathon, B.R. England, E.W. StClair, T. Arayssi, K. Carandang, K. D. Deane, M. Genovese, K.K. Huston, G. Kerr, et al., American college of rheumatology guideline for the treatment of rheumatoid arthritis, Arthritis Rheumatol. 73 (2021) 1108–1123, https://doi.org/10.1002/art.41752, 2021.
[11] I.A. Jones, R. Togashi, M.L. Wilson, N. Heckmann, C.T. Vangsness, Intra-articular treatment options for knee osteoarthritis, Nat. Rev. Rheumatol. 15 (2019) 77–90, https://doi.org/10.1038/s41584-018-0123-4.
[12] C.H. Evans, V.B. Kraus, L.A. Setton, Progress in intra-articular therapy, Nat. Rev. Rheumatol. 10 (2014) 12, https://doi.org/10.1038/nrrheum.2013.159.
[13] G. Neander, L.O. Eriksson, E. W»llin-Boll, H. Ersmark, A. Grahnen, Pharmacokinetics of intraarticular indomethacin in patients with osteoarthritis, Eur. J. Clin. Pharmacol. 42 (1992) 301–305, https://doi.org/10.1007/BF00266352.
[14] Q. Shen, Y. Du, A comprehensive review of advanced drug delivery systems for the treatment of rheumatoid arthritis, Int. J. Pharm. 635 (2023) 122698, https://doi.org/10.1016/j.ijpharm.2023.122698.
[15] V.B. Kraus, P.G. Conaghan, H.A. Aazami, P. Mehra, A.J. Kivitz, J. Lufkin, J. Hauben, J.R. Johnson, N. Bodick, Synovial and systemic pharmacokinetics (PK) of triamcinolone acetonide (TA) following intra-articular (IA) injection of an extended-release microsphere-based formulation (FX006) or standard crystalline suspension in patients with knee osteoarthritis (OA), Osteoarthr. Cartil. 26 (2018) 34–42, https://doi.org/10.1016/j.joca.2017.10.003.
[16] N. Bodick, J. Lufkin, C. Willwerth, R.C. Blanks, C.A. Inderjeeth, A. Kumar, M. D. Clayman, FX006 prolongs the residency of triamcinolone acetonide in the synovial tissues of patients with knee osteoarthritis, Osteoarthr. Cartil. 21 (2013) S144–S145, https://doi.org/10.1016/j.joca.2013.02.307.
[17] R.M. Stefani, A.J. Lee, A.R. Tan, S.S. Halder, Y. Hu, X.E. Guo, A.M. Stoker, G. A. Ateshian, K.G. Marra, J.L. Cook, et al., Sustained low-dose dexamethasone delivery via a PLGA microsphere-embedded agarose implant for enhanced osteochondral repair, Acta Biomater. 102 (2020) 326–340, https://doi.org/10.1016/j.actbio.2019.11.052.
[18] Y. Liang, J. Zhang, X. Zhao, M. Wang, S. Ding, Y. Wang, Y. Chen, J. Liu, Study on the slow-release mometasone furoate injection of PLGA for the treatment of knee arthritis, Curr. Drug Deliv. 18 (2021) 357–368, https://doi.org/10.2174/1567201817666200917124759.
[19] M. Janssen, U.T. Timur, N. Woike, T.J.M. Welting, G. Draaisma, M. Gijbels, L. W. van Rhijn, G. Mihov, J. Thies, P.J. Emans, Celecoxib-loaded PEA microspheres as an auto regulatory drug-delivery system after intra-articular injection, J. Contr. Release 244 (2016) 30–40, https://doi.org/10.1016/j.jconrel.2016.11.003.
[20] P. Arunkumar, S. Indulekha, S. Vijayalakshmi, R. Srivastava, Synthesis, characterizations, in vitro and in vivo evaluation of Etoricoxib-loaded poly (caprolactone) microparticles – a potential intra-articular drug delivery system for the treatment of osteoarthritis, J. Biomater. Sci. Polym. Ed. 27 (2016) 303–316, https://doi.org/10.1080/09205063.2015.1125564.
[21] I. Lamela-Gómez, L.M. Gonçalves, A.J. Almeida, A. Luzardo-Álvarez, Infliximab microencapsulation: an innovative approach for intra-articular administration of biologics in the management of rheumatoid Arthritis—in vitro evaluation, Drug Delivery and Translational Research 13 (2023) 3030–3058, https://doi.org/10.1007/s13346-023-01372-1.
[22] P. Puebla, P. Pastoriza, E. Barcia, A. Fernández-Carballido, PEG-derivative effectively modifies the characteristics of indomethacin-PLGA microspheres destined to intra-articular administration, J. Microencapsul. 22 (2005) 793–808, https://doi.org/10.1080/02652040500273902.
[23] A. Bernardi, A. Zilberstein, E. Jäger, M. Campos, F. Morrone, J. Calixto, A. Pohlmann, S. Guterres, A. Battastini, Effects of indomethacin-loaded nanocapsules in experimental models of inflammation in rats, Br. J. Pharmacol. 158 (2009) 1104–1111, https://doi.org/10.1111/j.1476-5381.2009.00244.x.
[24] N. Yin, X. Guo, R. Sun, H. Liu, L. Tang, J. Gou, T. Yin, H. He, Y. Zhang, X. Tang, Intra-articular injection of indomethacin–methotrexate in situ hydrogel for the synergistic treatment of rheumatoid arthritis, J. Mater. Chem. B 8 (2020) 993–1007, https://doi.org/10.1039/c9tb01795j.
[25] J.X. Zhang, M.Q. Yan, X.H. Li, L.Y. Qiu, X.D. Li, X.J. Li, Y. Jin, K.J. Zhu, Local delivery of Indomethacin to arthritis-bearing rats through polymeric micelles based on amphiphilic polyphosphazenes, Pharm. Res. 24 (2007) 1944–1953, https://doi.org/10.1007/s11095-007-9322-4.
[26] I. Guermech, M.A. Lassoued, A. Abdelhamid, S. Sfar, Development and assessment of lipidic nanoemulsions containing sodium hyaluronate and Indomethacin, AAPS PharmSciTech 20 (2019) 330, https://doi.org/10.1208/s12249-019-1543-4.
[27] M.J. Ho, S.R. Kim, Y.W. Choi, M.J. Kang, Recent advances in intra-articular drug delivery systems to extend drug retention in joint, Journal of Pharmaceutical Investigation 49 (2019) 9–15, https://doi.org/10.1007/s40005-018-0383-7.
[28] J. Pradal, M.-F. Zuluaga, P. Maudens, J.-M. Waldburger, C.A. Seemayer, E. Doelker, C. Gabay, O. Jordan, E. Allémann, Intra-articular bioactivity of a p38 MAPK inhibitor and development of an extended-release system, Eur. J. Pharm. Biopharm. 93 (2015) 110–117, https://doi.org/10.1016/j.ejpb.2015.03.017.
[29] J. Pradal, P. Maudens, C. Gabay, C.A. Seemayer, O. Jordan, E. Allémann, Effect of particle size on the biodistribution of nano- and microparticles following intra-articular injection in mice, Int. J. Pharm. 498 (2016) 119–129, https://doi.org/10.1016/j.ijpharm.2015.12.015.
[30] I.C.o. Harmonisation, ICH Harmonised Guideline, Validation Anal. Procedures Q2 (R2) (2023).
[31] Y. Kim, H. Sah, Protein loading into spongelike PLGA microspheres, Pharmaceutics 13 (2021), https://doi.org/10.3390/pharmaceutics13020137.
[32] T. Starr, T.J. Bauler, P. Malik-Kale, O. Steele-Mortimer, The phorbol 12-myristate-13-acetate differentiation protocol is critical to the interaction of THP-1 macrophages with Salmonella Typhimurium, PLoS One 13 (2018) e0193601, https://doi.org/10.1371/journal.pone.0193601.
[33] M.E. Lund, J. To, B.A. O'Brien, S. Donnelly, The choice of phorbol 12-myristate 13-acetate differentiation protocol influences the response of THP-1 macrophages to a pro-inflammatory stimulus, J. Immunol. Methods 430 (2016) 64–70, https://doi.org/10.1016/j.jim.2016.01.012.
[34] M. Otsuka, F. Kato, Y. Matsuda, Y. Ozaki, Comparative determination of polymorphs of indomethacin in powders and tablets by chemometrical near-infrared spectroscopy and X-ray powder diffractometry, AAPS PharmSciTech 4 (2003) 58–69, https://doi.org/10.1208/pt040219.
[35] J.M. Bezemer, D.W. Grijpma, P.J. Dijkstra, C.A. van Blitterswijk, J. Feijen, A controlled release system for proteins based on poly(ether ester) block-copolymers: polymer network characterization, J. Contr. Release 62 (1999) 393–405, https://doi.org/10.1016/S0168-3659(99)00170-4.
[36] A.A. Deschamps, Segmented Poly(Ether Ester)S and Poly(Ether Ester Amide)S for Use in Tissue Engineering, University of Twente, Enschede, 2002. PhD Thesis.
[37] S. Fakirov, A.A. Apostolov, P. Boeseke, H.G. Zachmann, Structure of segmented poly (ether ester)s as revealed by synchrotron radiation, J. Macromol. Sci. B 29 (1990) 379–395, https://doi.org/10.1080/00222349008230378.
[38] M.C. Gaspar, A.A.C.C. Pais, J.J.S. Sousa, J. Brillaut, J.-C. Olivier, Development of levofloxacin-loaded PLGA microspheres of suitable properties for sustained pulmonary release, Int. J. Pharm. 556 (2019) 117–124, https://doi.org/10.1016/j.ijpharm.2018.12.005.
[39] E. Atef, H. Chauhan, D. Prasad, D. Kumari, C. Pidgeon, Quantifying solid-state mixtures of Crystalline indomethacin by Raman spectroscopy comparison with thermal analysis, ISRN Chromatography 2012 (2012) 892806, https://doi.org/10.5402/2012/892806.
[40] S.R. Abulateefeh, A.M. Alkilany, Synthesis and characterization of PLGA shell microcapsules containing aqueous cores prepared by internal phase separation, AAPS PharmSciTech 17 (2016) 891–897, https://doi.org/10.1208/s12249-015-0413-y.
[41] K. Park, A. Otte, F. Sharifi, J. Garner, S. Skidmore, H. Park, Y.K. Jhon, B. Qin, Y. Wang, Potential roles of the glass transition temperature of PLGA microparticles in drug release kinetics, Mol. Pharm. 18 (2021) 18–32, https://doi.org/10.1021/acs.molpharmaceut.0c01089.
[42] M. Klepić, A. Fuoco, M. Monteleone, E. Esposito, K. Friess, Z. Petrusová, P. Izák, J. C. Jansen, Tailoring the thermal and mechanical properties of PolyActiveTM Poly (Ether-Ester) multiblock copolymers via blending with CO2-Phylic ionic liquid, Polymers 12 (2020), https://doi.org/10.3390/polym12040890.
[43] A.A. Deschamps, D.W. Grijpma, J. Feijen, Poly(ethylene oxide)/poly(butylene terephthalate) segmented block copolymers: the effect of copolymer composition on physical properties and degradation behavior, Polymer 42 (2001) 9335–9345, https://doi.org/10.1016/s0032-3861(01)00453-0.
[44] I. Carmagnola, T. Nardo, P. Gentile, C. Tonda-Turo, C. Mattu, S. Cabodi, P. Defilippi, V. Chiono, Poly(Lactic Acid)-Based blends with tailored physicochemical properties for tissue engineering applications: a case study, Int. J. Polym. Mater. Polym. Biomat. 64 (2015) 90–98, https://doi.org/10.1080/00914037.2014.886247.
[45] A. Prudic, A.-K. Lesniak, Y. Ji, G. Sadowski, Thermodynamic phase behaviour of indomethacin/PLGA formulations, Eur. J. Pharm. Biopharm. 93 (2015) 88–94, https://doi.org/10.1016/j.ejpb.2015.01.029.
[46] A.A. Öztürk, E. Yenilmez, M.G. Özarda, Clarithromycin-loaded poly (lactic-co-glycolic acid) (PLGA) nanoparticles for oral administration: effect of polymer molecular weight and surface modification with chitosan on formulation, nanoparticle characterization and antibacterial effects, Polymers 11 (2019), https://doi.org/10.3390/polym11101632.
[47] A.F. Girão, P. Wieringa, S.C. Pinto, P.A.A.P. Marques, S. Micera, R. van Wezel, M. Ahmed, R. Truckenmueller, L. Moroni, Ultraviolet functionalization of electrospun scaffolds to activate fibrous runways for targeting cell adhesion, Front. Bioeng. Biotechnol. 7 (2019) 159, https://doi.org/10.3389/fbioe.2019.00159.
[48] G. Kasten, K. Nouri, H. Grohganz, T. Rades, K. Löbmann, Performance comparison between crystalline and co-amorphous salts of indomethacin-lysine, Int. J. Pharm. 533 (2017) 138–144, https://doi.org/10.1016/j.ijpharm.2017.09.063.
[49] S.-Y. Lin, H.-L. Lin, Y.-T. Chi, R.-Y. Hung, Y.-T. Huang, C.-Y. Kao, W.-H. Hsieh, Povacoat affecting solid-state polymorphic changes of indomethacin after co-evaporation from different types of solvents via conventional and microwave drying techniques, Asian J. Pharm. Sci. 11 (2016) 376–384, https://doi.org/10.1016/j.ajps.2015.09.005.

[50] Y. Otsuka, W. Kuwashima, Y. Tanaka, Y. Yamaki, Y. Shimada, S. Goto, Effects of heat treatment on Indomethacin-Cimetidine mixture; investigation of drug-drug interaction using singular value decomposition in FTIR spectroscopy, J. Pharmaceut. Sci. 110 (2021) 1142–1147, https://doi.org/10.1016/j.xphs.2020.09.049.

[51] A.V. Ewing, G.S. Clarke, S.G. Kazarian, Stability of indomethacin with relevance to the release from amorphous solid dispersions studied with ATR-FTIR spectroscopic imaging, Eur. J. Pharm. Sci. 60 (2014) 64–71, https://doi.org/10.1016/j.ejps.2014.05.001.

[52] J.M. Bezemer, R. Radersma, D.W. Grijpma, P.J. Dijkstra, J. Feijen, C.A. van Blitterswijk, Zero-order release of lysozyme from poly(ethylene glycol)/poly (butylene terephthalate) matrices, J. Control. Release 64 (2000) 179–192, https://doi.org/10.1016/S0168-3659(99)00127-3.

[53] R.A. Graves, D. Poole, R. Moiseyev, L.A. Bostanian, T.K. Mandal, Encapsulation of Indomethacin using coaxial ultrasonic atomization followed by solvent evaporation, Drug Dev. Ind. Pharm. 34 (2008) 419–426, https://doi.org/10.1080/03639040701662636.

[54] J. Sohier, R. van Dijkhuizen-Radersma, K. de Groot, J.M. Bezemer, Release of small water-soluble drugs from multiblock copolymer microspheres: a feasibility study, Eur. J. Pharm. Biopharm. 55 (2003) 221–228, https://doi.org/10.1016/S0939-6411(02)00161-3.

[55] R. van Dijkhuizen-Radersma, S. Métairie, J.R. Roosma, K. de Groot, J.M. Bezemer, Controlled release of proteins from degradable poly(ether-ester) multiblock copolymers, J. Control. Release 101 (2005) 175–186, https://doi.org/10.1016/j.jconrel.2004.08.014.

[56] M. Butler, J.J. Boyle, J.J. Powell, R.J. Playford, S. Ghosh, Dietary microparticles implicated in Crohn's disease can impair macrophage phagocytic activity and act as adjuvants in the presence of bacterial stimuli, Inflamm. Res. 56 (2007) 353–361, https://doi.org/10.1007/s00011-007-7068-4.

[57] A.-M. Torché, P. Le Corre, E. Albina, R. Le Verge, PLGA microspheres phagocytosis by pig Alveolar macrophages: influence of Poly(vinyl alcohol) concentration, Nature of loaded-protein and copolymer nature, J. Drug Target. 7 (1999) 343–354, https://doi.org/10.3109/10611869909085517.

[58] P. Pacheco, D. White, T. Sulchek, Effects of microparticle size and Fc density on macrophage phagocytosis, PLoS One 8 (2013) e60989, https://doi.org/10.1371/journal.pone.0060989.

[59] D.M. Richards, R.G. Endres, How cells engulf: a review of theoretical approaches to phagocytosis, Rep. Prog. Phys. 80 (2017) 126601, https://doi.org/10.1088/1361-6633/aa8730.

[60] G.J. Cannon, J.A. Swanson, The macrophage capacity for phagocytosis, J. Cell Sci. 101 (1992) 907–913, https://doi.org/10.1242/jcs.101.4.907.

[61] J.-L. Davignon, M. Hayder, M. Baron, J.-F. Boyer, A. Constantin, F. Apparailly, R. Poupot, A. Cantagrel, Targeting monocytes/macrophages in the treatment of rheumatoid arthritis, Rheumatology 52 (2013) 590–598, https://doi.org/10.1093/rheumatology/kes304.

[62] X. Yang, Y. Chang, W. Wei, Emerging role of targeting macrophages in rheumatoid arthritis: focus on polarization, metabolism and apoptosis, Cell Prolif. 53 (2020) e12854, https://doi.org/10.1111/cpr.12854.

[63] J. Comer, S. Judge, D. Matthews, L. Towes, B. Falcone, J. Goodman, J. Dearden, The intrinsic aqueous solubility of indomethacin, ADMET and DMPK 2 (2014) 18–32, https://doi.org/10.5599/admet.2.1.33.

[64] D.E. Alonzo, G.G.Z. Zhang, D. Zhou, Y. Gao, L.S. Taylor, Understanding the behavior of amorphous pharmaceutical systems during dissolution, Pharm. Res. 27 (2010) 608–618, https://doi.org/10.1007/s11095-009-0021-1.

[65] M. Cutolo, A. Sulli, P. Ghiorzo, C. Pizzorni, C. Craviotto, B. Villaggio, Anti-inflammatory effects of leflunomide on cultured synovial macrophages from patients with rheumatoid arthritis, Ann. Rheum. Dis. 62 (2003) 297, https://doi.org/10.1136/ard.62.4.297.

[66] R. Thanan, M. Murata, N. Ma, O. Hammam, M. Wishahi, T. El Leithy, Y. Hiraku, S. Oikawa, S. Kawanishi, Nuclear localization of COX-2 in relation to the expression of stemness markers in urinary bladder cancer, Mediat. Inflamm. 2012 (2012) 165879, https://doi.org/10.1155/2012/165879.

[67] A.R. Abdollahi, F. Firouzian, R. Haddadi, A. Nourian, Indomethacin loaded dextran stearate polymeric micelles improve adjuvant-induced arthritis in rats: design and in vivo evaluation, Inflammopharmacology 29 (2021) 107–121, https://doi.org/10.1007/s10787-020-00776-6.

[68] T.H. Page, J.J.O. Turner, A.C. Brown, E.M. Timms, J.J. Inglis, F.M. Brennan, B.M. J. Foxwell, K.P. Ray, M. Feldmann, Nonsteroidal anti-inflammatory drugs increase TNF production in rheumatoid synovial membrane cultures and whole blood, J. Immunol. 185 (2010) 3694, https://doi.org/10.4049/jimmunol.1000906.

[69] M. Spatafora, G. Chiappara, D. D'Amico, D. Volpes, M. Melis, E. Pace, A. Merendino, Effect of indomethacin on the kinetics of tumour necrosis factor alpha release and tumour necrosis factor alpha gene expression by human blood monocytes, Pharmacol. Res. 23 (1991) 247–257, https://doi.org/10.1016/S1043-6618(05)80084-2.